A Quantitative Analysis of Cardiac Myocyte Relaxation: A Simulation Study

S. A. Niederer, P. J. Hunter, and N. P. Smith
Bioengineering Institute and Department of Engineering Science, The University of Auckland, Auckland, New Zealand

ABSTRACT The determinants of relaxation in cardiac muscle are poorly understood, yet compromised relaxation accompanies various pathologies and impaired pump function. In this study, we develop a model of active contraction to elucidate the relative importance of the $[Ca^{2+}]_i$ transient magnitude, the unbinding of Ca^{2+} from troponin C (TnC), and the length-dependence of tension and Ca^{2+} sensitivity on relaxation. Using the framework proposed by one of our researchers, we extensively reviewed experimental literature, to quantitatively characterize the binding of Ca^{2+} to TnC, the kinetics of tropomyosin, the availability of binding sites, and the kinetics of crossbridge binding after perturbations in sarcomere length. Model parameters were determined from multiple experimental results and modalities (skinned and intact preparations) and model results were validated against data from length step, caged Ca^{2+}, isometric twitches, and the half-time to relaxation with increasing sarcomere length experiments. A factorial analysis found that the $[Ca^{2+}]_i$ transient and the unbinding of Ca^{2+} from TnC were the primary determinants of relaxation, with a fivefold greater effect than that of length-dependent maximum tension and twice the effect of tension-dependent binding of Ca^{2+} to TnC and length-dependent Ca^{2+} sensitivity. The affects of the $[Ca^{2+}]_i$ transient and the unbinding rate of Ca^{2+} from TnC were tightly coupled with the effect of increasing either factor, depending on the reference $[Ca^{2+}]_i$ transient and unbinding rate.

INTRODUCTION

With each beat, the heart pumps blood around the body. The cyclical activation and relaxation of tension that takes place occurs at the sarcomere spatial scale and is controlled by cellular mechanisms. Each sarcomere is made up of interdigitated protein filaments of actin and myosin. Crossbridges protruding from myosin bind to actin, whereupon they undergo a conformational change, causing the bound crossbridges to pull each filament in opposite directions, producing tension. The process is controlled by both the local free Ca^{2+} and the intrinsic properties of the sarcomeres themselves.

Contraction is initiated by an increase in local $[Ca^{2+}]_i$. Ca^{2+} binds to troponin C (TnC) and the resulting shift of tropomyosin reveals the actin binding sites, allowing crossbridges to bind and generate tension. After the removal of $[Ca^{2+}]_i$, bound Ca^{2+} unbinds from TnC, tropomyosin blocks the actin binding sites, crossbridges detach, and tension returns to zero. The above processes producing the initiation of contraction in cardiac muscle are extensively quantified; however, the equally important mechanisms governing relaxation after contraction are poorly characterized. Thus although the steps are known in the process of relaxation, what controls each step and which step is the most important is unknown.

Relaxation is often quantified by the half-time to relaxation (RT_{50} the time for tension to decay by 50% from the peak value). RT_{50} is determined by both the $[Ca^{2+}]_i$ transient and the intrinsic properties of the myofilaments. The $[Ca^{2+}]_i$ transient influences RT_{50} when altered pharmacologically (1,2) or by increasing the stimulation frequency (3). The myofilament properties implicated as determinants of RT_{50} include the tension-dependent binding of Ca^{2+} to TnC (4), inhomogeneous sarcomere shortening (5), crossbridges inhibiting tropomyosin returning to its resting state (4), phosphorylation of troponin I (6), and sarcomere length (*SL*) (7). Unraveling the relative influences of each mechanism has proven challenging experimentally. In this study, we address this issue by unifying experimental data into a mathematical model to analyze the significant factors determining relaxation.

Building on the successful approach of cardiac electrophysiology models, cardiac contraction models are now beginning to quantify numerous phenomena, which have previously been poorly defined or only understood and characterized in isolation. Models of cardiac contraction have quantified cooperative mechanisms (8), the effects of contraction in the forward problem of electrocardiography (9), and ventricular pacing on contraction (10), for example. However, the parameters used in active contraction models are often derived from limited sets of experimental results. Here, each parameter was rationalized from numerous sources, and where possible, multiple experimental modalities, through an extensive review of the literature. The sources of each parameter and a brief description of the experimental conditions under which it was obtained are provided in the Tables.

The model is depicted in Fig. 1 and was based on the framework proposed by Hunter et al. (11). The equations and the parameters are described in the following stages:

Submitted July 26, 2005, and accepted for publication November 14, 2005.

Address reprint requests to S. A. Niederer, E-mail: s.niederer@auckland.ac.nz.

0006-3495/06/03/1697/26 $2.00
doi: 10.1529/biophysj.105.069534

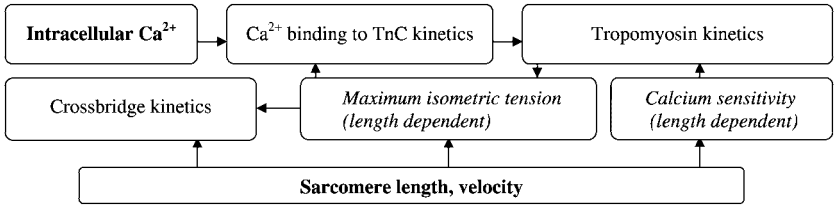

FIGURE 1 Flow diagram depicting the relationships of the active contraction framework proposed by Hunter et al. (11). The model is driven by *SL* and sarcomere velocity, and intracellular $[Ca^{2+}]_i$. Inputs are in bold, algebraic length dependencies are in italics, processes described by differential equations are standard font.

1. The kinetics of Ca^{2+} binding to TnC in the absence, and then presence, of tension was defined using steady-state and transient experimental data.
2. The shift in tropomyosin (Tm) to reveal the actin binding sites resulting from Ca^{2+} binding to TnC was characterized using light-activated Ca^{2+} chelator experiments and force-Ca^{2+} (F-pCa) curves.
3. Active tension was defined by the product of the available actin sites, the maximum isometric tension, and a sarcomere velocity-dependent scalar. Available actin sites were calculated from Tm kinetics. Maximum isometric tension was described by a linear function of *SL*, with parameters for this component defined by the maximum velocity, rapid length step, and sinusoidal perturbation experimental results.

The model was validated using rapid length-step experiments, caged Ca^{2+} tension transients, clamped and unclamped *SL* tension traces, and RT_{50} as a function of *SL*.

TROPONIN

Steady-state Ca^{2+} binding to troponin

The ternary cardiac troponin complex (Tn) consists of three subunits: Troponin I, T, and C. TnC contains the regulatory Ca^{2+} binding site, where the binding of Ca^{2+} initiates contraction. Troponin I (TnI) inhibits actin-myosin interaction. Troponin T (TnT) plays a structural role binding to TnC, TnI, and Tropomyosin (Tm) (12). TnC consists of N- and C-terminal globular lobes and is connected by a long central helix. The C-terminal contains binding sites III and IV, which bind Ca^{2+} and magnesium competitively. Under physiological conditions, both sites III and IV are saturated. The N-terminal contains Ca^{2+}specific or low-affinity binding sites I and II. In skeletal TnC, both sites are active; but in cardiac TnC, only site II is active, due to an increased positive charge near site I prohibiting the binding of Ca^{2+} (13). In cardiac TnC, site II regulates muscle contraction and is the focus of a large number of studies, due to its potential as a target for Ca^{2+}sensitizing drugs and its fundamental role in excitation-contraction coupling.

Steady-state Ca^{2+} binding to TnC can be described by a Hill equation with a Hill coefficient of 1 (Eq. 1) (14). Defining $[Ca^{2+}]_{Trpn}$ as the concentration of Ca^{2+} bound to TnC site II, $[Ca^{2+}]_{TrpnMax}$, as the maximum concentration of ions that can bind to site II, $[Ca^{+2}]_i$ is the concentration of free Ca^{2+} and K is the tension-dependent affinity of Ca^{2+} for TnC. K was determined initially from experimental results with zero or minimal tension (T) and the tension dependence is considered below. $[Ca^{2+}]_{TrpnMax}$ was set to 70 μM (15,16):

$$[Ca^{+2}]_{Trpn} = [Ca^{+2}]_{TrpnMax}\frac{[Ca^{+2}]_i}{[Ca^{+2}]_i + K(T)}. \quad (1)$$

Experimental measurements of Ca^{2+} affinity to site II are performed on a range of species and Tn subunits, under varying chemical conditions at different temperatures (see Table 1). The combinations of Tn subunits, Tm, and actin fundamentally affect the Ca^{2+} affinity of site II, as shown in Fig. 2. TnC in isolation has an affinity of $\approx$1 μM (13,17–25). TnC-TnI, Tn, and Tn-Tm have an affinity of $\approx$0.1 μM (13,21–23,26,27) Tn-Tm-Actin and skinned fibers have an affinity of $\approx$1 μM (22,27–31). However, outliers do exist in the literature: Fuchs and co-workers (32–34) did not differentiate between sites III and IV and site II affinities. Li and co-workers (18,24) measured affinities of 2.5 μM and 20 μM with whole TnC and the N-terminal of TnC containing site II, respectively, and found no evidence to rationalize the significant variation. Ball et al. (35) measured a higher affinity of Ca^{2+} to TnC, yet there does not appear to be a reason for this discrepancy. The effect of magnesium is varied between experiments, with magnesium having both minimal (13,23,36,37) and significant (25,29) effects; this may be due to differences in muscle or species types, as a significant difference is seen between rabbit skeletal and porcine cardiac muscle (29). Temperature, however, has only a minimal effect (17,30). Fuchs and co-workers (32–34,38–44) have shown that Ca^{2+} binding to Tn is dependent on active tension. In skinned preparations, bound crossbridges may play a role in determining the binding affinity. However, the majority of K-values were measured at low $[Ca^{2+}]$ ($<$2.5 μM) and so tension was assumed to be minimal (45,46). Ca^{2+} affinity values for Tn bound to actin lie between 0.83 μM (28) and 5 μM (22) using scintillation counting and IAANS florescence with cysteine (Cys) 35 in place, respectively. It has been suggested that IAANS results where the Cys amino acid located at residue 35 has been removed are more accurate than when Cys-35 is present (22). IAANS results with Cys-35 removed record affinities of 1.6–2.3 μM (22,29) and scintillation counting recorded affinities of 2.5 μM (27) and 2.0 μM (47) for TnC in whole fibers;

TABLE 1 Binding affinities of Ca^{2+} to site II of cardiac troponin C

Species	Temp (°C)	Troponin complex	Bound Ca^{2+} measure	Mg (mM)	K_d (M^{-1})	K (μM)	Ref.
Human	30	NTnC	NMRs	—	4×10^5	2.5	(18)
Human	15	TnC	F27W	None	4.2×10^4	24	(25)
Human	15	TnC	F27W	3	1.4×10^5	7.1	(25)
Human	30	TnC	NMRs	—	5×10^4	20	(24)
Bovine	4	TnC	SC	None	2.5×10^5	4.0	(13)
Bovine	4	TnC	SC	4	2.5×10^5	4.0	(13)
Bovine	—	TnC	IAANS	3	7×10^5	1.4	(35)
Bovine	7	TnC	F27W	—	9.3×10^4	11	(17)
Bovine	21	TnC	F27W	—	1.9×10^5	5.3	(17)
Bovine	37	TnC	F27W	—	2.6×10^5	3.9	(17)
Mammal	RT	TnC	IAANS	3	2.5×10^5	4.0	(23)
Mammal	RT	TnC	IAANS	None	4.5×10^5	2.2	(23)
Mammal	21	TnC	F27W	None	2×10^5	5.0	(19)
Rat	4	TnC	IAANS (84)	3	3.2×10^5	3.1	(20)
R/B	23	TnC	IAANS	3	7.2×10^5	1.4	(21)
Chicken	23	TnC	IAANS (84)	None	2.9×10^5	3.5	(22)
Chicken	23	TnC	IAANS	None	3.6×10^5	2.8	(22)
Chicken	23	TnC-TnI	IAANS (84)	5	8×10^5	1.3	(22)
Bovine	—	TnC-TnI	IAANS	3	1.5×10^7	0.07	(35)
Rat	—	TnC-TnI	IAANS	3	1.7×10^6	0.59	(26)
R/B	23	TnC-TnI	IAANS	3	1.5×10^6	0.67	(21)
Mammal	RT	TnC-TnI	IAANS	None	3×10^6	0.33	(23)
Bovine	4	TnC-TnI	SC	4	1×10^6	1.0	(13)
Bovine	4	TnC-TnI	SC	None	1×10^6	1.0	(13)
Chicken	23	Tn	IAANS	5	1.2×10^6	0.83	(22)
Bovine	4	Tn	SC	None	2.5×10^6	0.40	(13)
Bovine	4	Tn	SC	4	2.5×10^6	0.40	(13)
Bovine	25	Tn-Tm	IAANS	2.5	1.2×10^6	0.83	(27)
P/C*	RT	SP	IAANS (84)	1	6.3×10^5	1.6	(29)
R/C	RT	SP	IAANS (84)	1	6.3×10^5	1.6	(29)
Bovine	25	SP	SC	5	$4 \times 10^{6\dagger}$	0.25	(33)
Bovine	25	SP	SC	5	$2 \times 10^{6\dagger}$	0.50	(32)
Bovine‡	25	Tn-Tm-A	SC	2.5	4×10^5	2.5	(27)
Bovine	25	Tn-Tm-A	SC	2.5	9.6×10^5	1.0	(27)
Bovine	25	Tn-Tm-A	IAANS	2.5	1.1×10^6	0.91	(27)
Bovine	25	SP	SC	5	$2 \times 10^{6\dagger}$	0.5	(34)
R/C	23	SP	IAANS	1	2×10^5	0.5	(22)
R/C	23	SP	IAANS (84)	1	4.7×10^5	2.1	(22)
Canine	25	SP	SC	2, 10	1.2×10^6	0.83	(28)
Canine	25	SP	SC	2	2.36×10^5	4.2	(31)

IAANS is IAANS-labeled TnC; *IAANS* (*84*) is IAANS-labeled TnC, with Cys amino acids at residue 84; *NMRs* is NMR spectroscopy; *None* = $<1 \times 10$–3 mM; *P/C* is porcine fiber with chicken TnC; *R/B* is rat fiber/bovine Tn-Tm; *R/C* is rat fiber with chicken TnC; *SC* is scintillation counting; and *SP* is skinned preparation. *RT* is room temperature.

*BDM added.

†Affinity for sites II, III, and IV combined.

‡IAANS bound, but not used to measure affinity.

therefore the binding affinity of TnC (K) contained in whole fibers was set to be 2 μM in the absence of tension. This value was used in the model and the allosteric affects, if any, of magnesium binding were assumed to be minimal.

Ca^{2+} binding kinetics

Equation 2 defines the kinetic binding of Ca^{2+} to site II in TnC was proposed by Robertson et al. (14). The value k_{on} is the rate of binding and k_{off} is the tension-dependent rate of unbinding of Ca^{2+} from TnC. Equation 1 is the steady-state solution to Eq. 2 with $K = k_{off}/k_{on}$:

$$\frac{d[Ca^{2+}]_{Trpn}}{dt} = k_{on}[Ca^{2+}]_i([Ca^{2+}]_{TrpnMax} - [Ca^{2+}]_{Trpn}) - k_{off}(T)[Ca^{2+}]_{Trpn}. \quad (2)$$

Large variations are seen in the reported unbinding rates of Ca^{2+} from site II (k_{off}). Temperature does not appear to have a significant affect on the unbinding rate. The rate lies between 1.3 s^{-1} and 750 s^{-1} at 4°C, 17 s^{-1}, and 1200 s^{-1} at 15°C, and 13 s^{-1} and 900 s^{-1} at room temperature. It is important to again note that there is significant variation in the binding affinity (K) of Ca^{2+} for TnC for different combinations of Tn subunits, Tm, and actin, as outlined in the

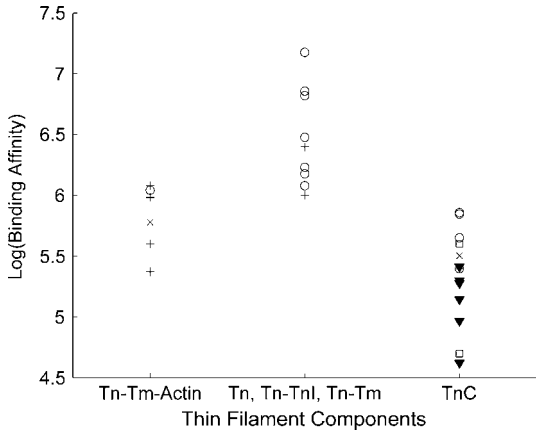

FIGURE 2 Affinity of Ca^{2+} to TnC contained in various components of mammalian cardiac thin filaments, from studies listed in Table 1. The plus-symbol (+) is scintillation counting; ○ is IAANS (Cys-35, Cys-84); × is IAANS (Cys-35); ▼is F27W; and □ is MRI spectroscopy.

above section (see Fig. 2). The variation in K will be reflected in the kinetics by a change in the ratio of unbinding and binding rates with different combinations of Tn complexes. Unbinding rates for TnC bound to Tn-Tm, Tn-TnI, and Tn are in the order of $\approx$10 s^{-1} (47–49), which coincide with the higher reported affinities for the same Tn complexes (*center column* of Fig. 2). TnC in isolation has varied unbinding rates between 11 s^{-1} and 5000 s^{-1} and a lower binding affinity (illustrated in the *right column* of Fig. 2). The majority of binding rates lie within a factor of 2 of 100 μM^{-1} s^{-1} (20,25,48,50–53) (see Table 2) with no apparent variation between temperatures or combinations of Tn subunits and Tm. Binding and unbinding rates have not been measured in whole fiber preparations. To determine the rates in whole fibers, it was assumed that it was primarily the unbinding rate, and not the binding rate, which changes for different TnC complexes, resulting in the changes in binding affinity (K) reported above. This assumption is consistent with the hypothesis that binding of Ca^{2+} to site II is diffusion-limited (54). The binding rate was set to 100 μM^{-1} s^{-1}, and using the affinity of Ca^{2+} for TnC derived above from Table 1 of 2 μM, the unbinding rate for site II of TnC contained in Tn-Tm-actin was $k_{off} = K \cdot k_{on} = 200$ s^{-1}.

Tension-dependent Ca^{2+} unbinding rate from Troponin C

The tension-dependent binding of Ca^{2+} to TnC has been elucidated via a number of discrete experimental techniques. The affinity of Ca^{2+} for TnC decreases during rapid step-length reduction experiments on intact muscle (55–57). The concentration of Ca^{2+} bound to TnC decreases when tension development is inhibited with vanadium (33,40). Modeling experiments using Ca^{2+}-sensitizing drugs indicate that Ca^{2+} binding to TnC is likely to be tension-dependent (58). The tension-dependent unbinding rate from Eq. 2 is defined by Eq. 3, below. The form of Eq. 3 captures tension-dependent components of Ca^{2+} binding to site II of TnC as well as the length-dependent components, as discussed below.

$$k_{off} = k_{refoff}\left(1 - \frac{T}{\gamma T_{ref}}\right), \tag{3}$$

where k_{refoff} is the unbinding rate in the absence of tension, γ is a measure of the affect of tension on the unbinding rate, T is the active tension, and T_{ref} is the reference tension (described below). The value γ is not measured directly experimentally but can be calculated using results from Ca^{2+}

TABLE 2 Binding and unbinding rates of Ca^{2+} to site II in TnC

Species	Muscle	Temp (°C)	Troponin complex	Bound Ca^{2+} measure	K_{on} (μM^{-1} s^{-1})	K_{off} (s^{-1})	Ref.
Rabbit	S	4	TnC	F29W	100–200	—	(50)
Rabbit	S	4	TnC	DANZ	100–200	—	(50)
Rabbit	S	15	TnC	F29W	100	340	(51)
Rabbit	S	22	TnC	F29W	—	350	(50)
Rabbit	S	22	TnC	DANZ	—	551	(50)
Rabbit	S	22	TnC	Quin-2	290	462	(50)
Human	C	4	TnC	IAANS	—	73	(52)
Human	C	15	TnC	F27W	170	1159–1263	(25)
Human	C	20	TnC	IAANS	100	483	(52)
Human	C	30	TnC	NMRs	250	5000	(24)
Bovine	C	4	TnC	IAANS	51	11	(48)
Bovine	C	15	TnC	Quin-2	—	136.5	(49)
Chicken	C	4	TnC	Quin-2, BAPTA	200–400	700–800	(53)
Rat	C	4	TnC	IAANS	140	437	(20)
Bovine	C	4	TnC-TnI	IAANS	59	12	(48)
Bovine	C	15	Tn-Tm	IANDB	—	16.2–18.2	(49)
Bovine	C	15	Tn-Tm	Quin-2	—	23	(49)
Chicken	S	4	Tn-Tm	IANDB	10	1.3	(47)
Chicken	S	20	Tn-Tm	IANDB	65	13	(47)
Model	C	N/A	SP	—	39	19.6	(14)

C is cardiac; *S* is skeletal.

affinity and length-step experiments in skinned and intact preparations, respectively. As now discussed, calculating γ in both intact and skinned preparations confirms that the tension-dependent binding of Ca^{2+} to TnC is not affected by the skinning process.

Fuchs and co-workers have shown that the concentration of bound Ca^{2+} is both tension- (33,40,44) and length-dependent (32,38,40,42,44) in skinned preparations. However, it is likely that these two dependencies are related by the number of attached crossbridges (55), which increases with length (59) and has been shown to increase the binding affinity of Ca^{2+} for TnC (47). The tension dependence of Ca^{2+} binding to TnC is consistently supported by the results within individual experiments. Comparing results between experiments, however, reveals inconsistencies. In the absence of bound crossbridges due to the addition of vanadate, between ≈75% (33,40) and ≈50% (44) of site IIs are occupied at pCa = 5. It was then expected that, if tension were the only factor determining the binding of Ca^{2+} to TnC, then at pCa = 5, no less than 50–75% of sites should be occupied in the presence of tension, yet measurements of 35% (32), 49% (44), and 69% (42) of site IIs occupied at pCa 5 in the presence of tension have been reported. The variation can be rationalized by three potential mechanisms. Firstly, that some mechanism other than bound crossbridges affects affinity. Secondly, variations between preparations affected the results. Thirdly, the method used here to calculate the number of ions bound to site II introduces or increases variation in the measurements. Fuchs and co-workers measured the total concentration of Ca^{2+} bound to all three sites of TnC. As sites III and IV are known to have a higher affinity than site II it was assumed that they are both saturated at pCa 5. Therefore the fraction of site IIs occupied by Ca^{2+} is equal to the total number of ions bound per TnC molecule less two. As a result, the fraction of site IIs occupied by Ca^{2+} is sensitive to experimental noise. If, on average, a total of 2.8 ions are bound to TnC at pCa = 5, then a variation of 3.6% (32) in the total number of ions bound to TnC corresponds to a variation of 0.1 ions. Subtracting the two ions bound to the saturated sites III and IV from the total number of ions bound (2.8 ions) means that there is a 0.1 ion variation in the remaining 0.8 ions bound to site II, which corresponds to a 12.5% variation in the number of ions bound to site II. This amplification of the experimental noise potentially explains the variation in experimental results observed. The affinity of Ca^{2+} for TnC in the absence of tension derived from Table 1 was 2 μM, which corresponds to 83% of site IIs being occupied at pCa 5 in the absence of tension, comparable with measurements of ≈75% (33,40). The value γ was determined using the K-value in the absence of tension defined above and a subset of results from Table 3. Results from experiments where Dextran or Vanadate were added, when the average SL was outside the physiological range of 1.8–2.3 μm or when the fraction of bound Ca^{2+} is <83% at pCa 5 (the value defined by Eq. 1 at zero tension), were excluded from the subset. The final subset took results from Fuchs and co-workers (32,33,38,42,44); γ was determined for each measurement, and the average γ-value was 1.9.

TABLE 3 Ca^{2+} bound to bovine cardiac troponin C site II

Temp (°C)	Additives	Sarcomere length (μm)	Fraction of site II with bound Ca^{2+}	Ref.
22	None	1.5–1.6	0.49	(44)
22	None	1.7	0.83	(38)
—	None	1.7	0.69	(42)
RT	None	1.74	0.25	(40)
25	None	1.81	0.35	(32)
22	None	1.9	0.80	(43)
22	None	2.2–2.3	1	(44)
22	None	2.2–2.3	1	(44)
22	None	2.3	1	(38)
—	None	2.3	0.94	(42)
25	None	2.34	1	(32)
25	None	2–2.5	1	(33)
RT	None	2.45	1	(42)
22	2% dextran	2	1	(38)
22	5% dextran	1.7	1	(38)
—	5% dextran	1.7	1.0	(42)
—	5% dextran	2.3	1.0	(42)
22	5% dextran	1.9	1.0	(43)
22	10% dextran	1.9	0.80	(43)
22	15% dextran	1.9	0.26	(43)
25	1 mM Vi	2–2.5	0.74	(33)
RT	1 mM Vi	2.28–2.34	0.72	(40)
RT	1 mM Vi	1.52–1.78	0.72	(40)
22	1 mM Vi	2.2–2.3	0.50	(44)

RT is room temperature. Bound calcium is calculated using 0.34 μmol troponin/g of fiber. Bovine cardiac muscle at pCa5 is used in all cases. It is assumed that, at pCa 5.0, the high-affinity sites are saturated. If total calculated bound Ca^{2+} was >3, it is assumed that site II is saturated. It is assumed $T \approx T_0$ at pCa5, in the absence of any additives.

To ensure that the skinning procedure did not affect the tension dependence of K, skinned results were compared with intact values. In intact preparations, length-step experiments elucidate the value of γ. Results by Allen and Kentish (56), using the Ca^{2+} released during length step experiments, estimated that the affinity of Ca^{2+} for TnC (K) would halve when tension was dropped to zero during a length step corresponding to a γ-value of 2. Komukai et al. (57) found a linear relationship between $\Delta[Ca^{+2}]_i/[Ca^{+2}]_i$ (the ratio of the quantity of Ca^{2+} released during a step change to the free Ca^{2+} before a length change) with the tension before by the length change (T_1) as tension increased (see Eq. 4). The size of the length steps were defined such that the tension after the length change was equal to zero:

$$\frac{\Delta[Ca^{2+}]_i}{[Ca^{2+}]_i} = -0.0066T_1. \quad (4)$$

Equations 5 and 6 define the concentration of bound Ca^{2+} before and after the length-step change, respectively, using Eq. 1, and the Ca^{2+} affinity is an unknown function of tension $K(T)$,

$$[Ca^{2+}]_{Trpn} = [Ca^{2+}]_{TrpnMax}\frac{[Ca^{2+}]_i}{[Ca^{2+}]_i + K(T_1)}, \quad (5)$$

$$[Ca^{2+}]_{Trpn} - \Delta[Ca^{2+}]_i = [Ca^{2+}]_{TrpnMax} \times \frac{[Ca^{2+}]_i + \Delta[Ca^{2+}]_i}{[Ca^{2+}]_i + \Delta[Ca^{2+}]_i + K(T=0)}. \quad (6)$$

Combining Eqs. 5 and 6, and assuming $[Ca^{2+}]_{TrpnMax} \gg \Delta[Ca^{2+}]_i$ (56),

$$[Ca^{2+}]_i K(T_1) - K(T=0) \cdot ([Ca^{2+}]_i + \Delta[Ca^{2+}]_i) \approx 0. \quad (7)$$

Now the Ca^{2+} tension relationship defined in Eq. 4 can be used to transform Eq. 7 from a Ca^{2+}-dependence of K to a tension-dependence of K. Using Eq. 4 proposed by Komukai and $K(T = 0)$ is equal to the affinity of Ca^{2+} to site II in the absence of tension (K):

$$K(T_1) = K(T=0) \cdot \left(1 + \frac{\Delta[Ca^{2+}]_i}{[Ca^{2+}]_i}\right) = K(1 - 0.0066T_1). \quad (8)$$

Setting Eq. 8 equal to Eq. 3 divided by k_{on}, γ is equal to 2.6, using $T_{ref} = 56.2$ kPa. The calculated γ-value of 1.9 from Fuchs and co-workers for skinned preparations is close to calculated γ-values in length-step experiments in intact preparations and suggests that the skinning process has a minimal affect on the tension dependence of Ca^{2+} binding to TnC.

The Ca^{2+} affinity for TnC has also been shown to vary with *SL* (32,40,44). In length-step experiments, the affinity of TnC drops significantly but the *SL* remains largely unchanged. The γ -value required to capture this phenomenon is close to the γ-value required to model the change in calcium affinity at varying fixed *SL* values. Hence, the *SL* dependence of the affinity is accounted for by the tension dependence, as maximum tension and tension-based Ca^{2+} sensitivity increase with increasing *SL* (discussed below). This hypothesis coincides with experiments, where crossbridge heads (myosin subfragment 1) bound to actin in the absence of myosin or any reference length increased the binding affinity of Ca^{2+} for TnC (47). In the model, the length dependence is accounted for by the tension dependence and the form of the equation is validated by Komukai's results. Considering these results γ will be set to 2.

TROPOMYOSIN

Tropomyosin is a highly extended α-helical coil situated in the actin groove, with each tropomyosin molecule spanning seven actin monomers (27). When tropomyosin is shifted out of the actin groove, the steric hindrance preventing actin binding to myosin is removed, allowing tension to develop. In the model, tropomyosin was characterized by z, the fraction of actin sites available for crossbridge binding. In this study, it is assumed that crossbridges bind rapidly relative to thin filament kinetics and that not all actin sites are available at full activation. Thus, tension is proportional to z and the ratio of z to the fraction of actin sites available at full activation for a given *SL* (z/z_{Max}) is equal to the ratio of the isometric tension to the maximum tension at full activation for the same *SL* (T_0/T_{0Max}). The value z is defined by Eq. 9, below. The fraction of actin sites available at full activation (z_{Max}) is defined by Eq. 14, the steady-state solution to Eq. 9 at full activation ($[Ca^{2+}]_{Trpn} = [Ca^{2+}]_{TrpnMax}$). The value T_0 is the isometric tension at a given $[Ca^{2+}]_i$ and *SL* (see Eq. 16). The value T_{0Max} is the isometric tension at full activation for a given *SL* (see Eq. 15).

$$\frac{dz}{dt} = \alpha_0 \left(\frac{[Ca^{2+}]_{Trpn}}{[Ca^{2+}]_{Trpn50}}\right)^n (1-z) - \alpha_{r1} z - \alpha_{r2}\frac{z^{n_r}}{z^{n_r} + K_Z^{n_r}}, \quad (9)$$

where the relaxation kinetics in Eq. 9 are described by α_{r1} and α_{r2}, K_z and n_r, which correspond to the slow and fast relaxation rates, respectively, observed in light-activated Ca^{2+} chelator experiments. The tension transients produced in light-activated Ca^{2+} chelator experiments are potentially defined by three mechanisms—the $[Ca^{2+}]_i$ bound to TnC, crossbridge kinetics, or the intrinsic properties of tropomyosin. The rate that tension decreases is significantly slower than the rate that calcium disassociates from TnC and, as such, the rate of relaxation is unlikely to be defined by $[Ca^{2+}]_i$ bound to TnC. The rate that tension decreases after a step decrease in Ca^{2+} is similar between species (rat (60–63) and guinea pig (5,64,65)) exhibiting different myosin isoforms, suggesting that crossbred kinetics do not define relaxation rates. Palmer and Kentish observed significant differences between guinea pig and rat preparation relaxation rates of 16.1 s^{-1} and 2.99 s^{-1}, respectively. However, their results are inconsistent with other experimental observations, which have consistently reported guinea pig relaxation rates of 10 s^{-1} and above (5,64,65). As such, the intrinsic properties of tropomyosin are assumed to be defined by the tension transients after step decreases in calcium. The length-dependent activation kinetics are described by $[Ca^{2+}]_{Trpn50}$, α_0, and n. The value $[Ca^{2+}]_{Trpn50}$ is the Ca^{2+} bound to TnC at half-activation and was derived from the free Ca^{2+} at half-activation. The value α_0 describes the monoexponential activation rate seen in caged Ca^{2+} experiments. The value n is analogous to the Hill coefficient in the steady-state force Ca^{2+} curve (F-pCa) and provides a phenomenological representation of the high cooperativity, due to nearest-neighbor interactions between tropomyosin and/or crossbridges, seen in the activation of tension in cardiac muscle.

Tropomyosin kinetics are described in four stages, which were cyclically iterated through. Briefly, first, the relaxation parameters (α_{r1}, α_{r2}, K_z, and n_r) are defined using step changes in Ca^{2+} experiments. Secondly, length-dependent activation ($[Ca^{2+}]_{Trpn50}$) is defined using half-activation values from skinned preparations and the resulting equation

is scaled to match intact preparation data. Thirdly, α_0 and n are defined for skinned and intact preparations by fitting the steady-state solution of Eq. 9 to the respective F-pCa curves. Finally, z_{Max}—the fraction of actin sites available at maximum activation—is calculated using the steady-state solution to Eq. 9.

Relaxation parameters

The relaxation kinetics described by Eq. 9 propose two stages for relaxation, as seen experimentally. It was found that a linear component involving α_{r1} characterized the slow process and a nonlinear component in the form of a Hill relation was required to model the fast component. Using the combined linear and nonlinear off-rates, the biphasic nature of relaxation was captured. To compare model simulations with experimental results, the relative tension T_0/T_{0Max} (or equivalently, T/T_0 in experimental nomenclature) was calculated using $T_0/T_{0Max} = z/z_{Max}$, where z_{Max} is defined below by Eq. 14.

The relaxation components of Eq. 9 were fitted using the tension transient after a step decrease in free Ca^{2+} using the light-activated Ca^{2+} chelator diazo-2. Ca^{2+} disassociates rapidly from TnC after a step decrease in Ca_i^{2+} and was therefore expected to have a minimal affect, such that the relaxation kinetics of tropomyosin solely determine the tension transient. In Ca^{2+} step experiments the muscle is often removed from the bathing solution and exposed to a pulse of light, which greatly increases the affinity of diazo-2 for Ca^{2+}, causing a reduction of free Ca^{2+} on a millisecond timescale. Data from rat and guinea pig preparations were used with both similarities and dissimilarities between species being observed. Experiments are commonly performed in air at the due temperature to reduce the affects of evaporation or condensation. As such, most experiments are performed at 12–15°C with the exception of results from Kentish and Palmer (63,66), where the muscle was kept in the bathing solution at 20–22°C. Results from diazo-2 experiments are summarized in Table 4. A biphasic tension transient is observed in most experiments, which is fitted with two exponentials. The rates are ≈10–12 s^{-1} and ≈2–4 s^{-1}, respectively, at 12–15°C for rat and guinea pig (60,62,64,65); and ≈16–18 s^{-1} and ≈1 s^{-1} at 22°C for rat in two other studies, respectively (63,66). The sole anomaly was recorded by Saeki et al. (61), who reported a fast transient of 73.5 s^{-1}, six times larger than any other experiment. The subsequent article by the same group using similar methods did not record the higher transient rate, and made no reference to their earlier results (60). The tension transients recorded by Simnett et al. (65) at 20°C had a half-time to relaxation of 53.4 ms, approximately the same as the control rat measurements at 15°C from Fitzimons et al. (62), which had a half-time to relaxation of 64.5 ms. However, removing the muscle from the bath would result in a drop in temperature of 2–3°C (65), and during activation, ADP and P_i can build up in preparations removed from the bath (63), both of which would affect relaxation. Palmer and Kentish (63,66) recorded relaxation times using rat trabeculae contained in the bathing solution, reducing any buildup of P_i or ADP and attaining data at 22°C, but characteristic tension traces published by Palmer and Kentish had a maximum tension of ≈0.3 T_0. The relaxation parameters were chosen to fit experimental results from Saeki et al. (60) and Simnett et al. (65) at 12–15°C, since an accurate fit to all data was not possible with limited information on *SL* (6,64), relative amplitudes of fast and slow processes (62,66), and initial

TABLE 4 Light-activated calcium chelator tension relaxation transients

Species	Prep	Temp (°C)	Initial pCa	*SL* (μm)	T_1/T_0	T_2/T_0	P_1	$k_1(s^{-1})$	P_2	$k_2(s^{-1})$	Ref.
Rat	T	14–15	5.8	2.2	0.5	0.05	18.9	73.5	85.3	9.8	(61)
Rat	T	14–15	6.1	2.2	—	—	93	12.1	8	2	(60)
Rat	T	14–15	5.8	2.2	—	—	93	12.1	8	2	(60)
Rat	T	14–15	5.6	2.2	—	—	93	12.1	8	2	(60)
GP	T	12	—	2.2	1	0	49	10.0	51	4.23	(65)
GP	T	20	—	2.2	1	0	92	18.4	15	2.52	(65)
Rat	T	22	—	2.1	0.4	0.1	—	16.1	—	0.97	(66)
GP	T	22	—	2.1	0.61	0.33	—	2.99	—	—	(66)
GP	T	12	—	—	1	0	45	11.2	57	2.9	(64)
Rat	V	15	5.5	2.3	0.48	0	—	10.8*	—	—	(62)
Pig	V	—	—	—	0.8	0	—	6.3*	—	—	(6)
Rat	T	22	5.56	2.1	—	0	46	16.6	54	1.1	(63)
Rat	T	22	5.56	2.1	—	0	48	17.3	52	1.3	(63)
GP†‡	V	10	4.5	2.25–2.4	1	0	—	12	—	0.3	(5)
Mouse‡	V	10	4.5	2.25–2.4	1	0	—	18	—	1.8	(145)
GP‡	T	10	4.5	2.25–2.4	1	0	—	10.8	—	0.6	(145)
Human‡	T	10	4.5	2.25–2.4	1	0	—	4.6	—	0.15	(145)

SL is sarcomere length. *GP* is guinea pig. *T* is trabeculae; *V* is ventricle.

*Calculated from half-time of relaxation. [Ca^{2+}] was rapidly decreased using diazo-2.

†Stehle et al. (5,145) fitted a piecewise function containing a linear region with a slope equal to k_2 and an exponential region with rate k_1.

‡Used rapid solution changes to change [Ca^{2+}].

tension (63). Fig. 3 shows results from Saeki et al. (60) (*points*) and model simulations (*lines*) with α_{r1}, α_{r2}, K_z, and n_r equal to 2 s^{-1}, 1.75 s^{-1}, 0.15, and 3, respectively.

Activation parameters

Having defined the parameters corresponding to relaxation, the remaining parameters could be fitted using caged Ca^{2+} tension transient experiments or F-pCa curves. Caged Ca^{2+} experiments are principally performed over a narrow range of *SL*, inhibiting their ability to characterize any length dependence. F-pCa curves, which are performed over a wide range of *SL*s, are used to characterize the remaining parameters.

F-pCa curves were used to define steady-state z in the solution of Eq. 9 using the commonly fitted experimental relationship in Eq. 10. The F-pCa relationship was described by a Hill curve with half-activation $[Ca^{2+}]_{50}$ and Hill coefficient *nH*. These two variables are commonly recorded experimentally (see Table 5),

$$\frac{z}{z_{max}} = \frac{T_0}{T_{0max}} = \frac{[Ca^{2+}]_i^{nH}}{[Ca^{2+}]_i^{nH} + [Ca^{2+}]_{50}^{nH}}. \quad (10)$$

The activation parameters in Eq. 9 were defined using F-pCa curves in two parts. First, the length-dependent activation was defined by determining the length dependence of $[Ca^{2+}]_{Trpn50}$, which was calculated from the length-dependent $[Ca^{2+}]_{50}$ values defined in Eq. 10 from skinned and intact preparations by rearranging the equations outlined above. Secondly, α_0 and n were determined by fitting the steady-state solution to Eq. 9 to F-pCa curves. The F-pCa curves were defined by the half-activation values used to calculate $[Ca^{2+}]_{Trpn50}$ and Hill coefficients for skinned and intact preparations.

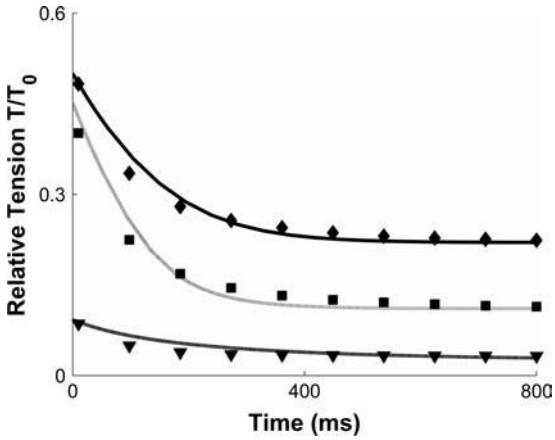

FIGURE 3 Relaxation after activation of Ca^{2+} chelator; data points from Saeki et al. (60), and lines are from model simulations. The ▼ data points and dashed line, ■ data points and dotted line, and ♦ data points and solid line had initial relative tensions of 0.5, 0.451, and 0.0925, respectively, and the pCa values after the activation of the calcium chelator were 5.78, 5.92, and 6.3, respectively. The pCa values were calculated using the final relative tensions and the skinned F-pCa curve defined below with a Hill coefficient of $n = 3$ and half-activation value of $pCa_{50} = 5.6$. $SL = 2.2$ μm.

Length-dependent activation

$[Ca^{2+}]_{50}$ is dependent on *SL*, which is seen as a leftward shift in the F-pCa curve as *SL* increases (67–70). The increased sensitivity has been associated with axial stretch (46), interfilament spacing (44), bound crossbridges kinetics (71), and titin (72). Fuchs et al. (38,42–44) and McDonald and Moss (73) found that fiber width predominantly determined length-dependent Ca^{2+} sensitivity. Then, using fiber width as an indicator of interfilament spacing, they concluded that interfilament spacing determined length-dependent Ca^{2+} sensitivity. Recently, Konhilas et al. (74) measured interfilament spacing using x-ray diffraction, and showed that fiber width is a poor indicator of interfilament spacing and that interfilament spacing does not affect length-dependent Ca^{2+} sensitivity. Moss and Fitzsimons (75), in their critical review of the results of Konhilas et al. (74), acknowledged the technical difficulties of the experiments and the potential for experimental error, but also believe that this does not detract from the fundamental finding that myofilament spacing is not the predominant cause of the length dependence of Ca^{2+} sensitivity. Unfortunately few other hypothesis exist to account for this phenomenon (75,76), though modeling results from Rice and de Tombe (76) suggest the possibility that cooperative effects between the regulatory units (troponin and tropomyosin) could account for increased Ca^{2+} sensitivity at longer *SL*s.

$[Ca^{2+}]_{Trpn50}$ is defined by Eq. 11, derived from Eq. 15 and Eq. 2, as a function of $[Ca^{2+}]_{50}$ values and strain. Eq. 15 is defined below, and describes the length dependence of isometric tension. Here it was used to define the ratio between T/T_{ref} from Eq. 2 as a function of strain:

$$[Ca^{+2}]_{Trpn50} = [Ca^{2+}]_{TrpnMax} \times \frac{[Ca^{2+}]_{50}}{[Ca^{2+}]_{50} + \frac{k_{reloff}}{k_{on}}\left(1 - \frac{(1+\beta_0(\lambda-1))\times 0.5}{\gamma}\right)}. \quad (11)$$

$[Ca^{2+}]_{50}$ values contained in Eqs. 11 and 10 were defined as a linear function of strain (see Eq. 12). Fig. 4 plots $[Ca^{2+}]_{50}$ values for measurements taken under physiological conditions at room temperature in Table 5 against strain. The length-dependent Ca^{2+} sensitivity was defined in terms of a linear fit to the Ca_{50} values. Data was taken predominantly from rats at room temperature under physiological conditions (45,66,77–84). Data was excluded on the grounds of extreme ($SL < 1.8$ μm, $SL > 2.3$ μm) or unstated *SL*s (57,77,85), low levels of ATP (<4 mM) (80), low ionic strength (86,87) (<180 mM), and low or unstated temperatures (46,79,88) (<20°C). Intact muscle experiments (2,3,89) are considered separately below. The relationship between $[Ca^{2+}]_{50}$ and strain is described by Eq. 12 with $[Ca^{2+}]_{50ref} = 4.72$ μM and $\beta_1 = -4.0$ in skinned preparations,

TABLE 5 Rat tension-free calcium sensitivity

Species	Muscle	Temp (°C)	Ionic strength	Mg^{2+} (mM)	ATP (mM)	Sarcomere length (μm)	pCa_{50}	n_1	n_2	Ref.
Rat	T	22–24	200	3	5	1.65	5.02	4.35	—	(45)
Rat	T	15	200	1	5	1.85	5.35	4.8	8.6	(46)
Rat	V	15	180	—	4.74	1.85	5.41	—	3.4	(71)
Rat	T	22–24	200	3	5	1.75	5.11	2.82	—	(45)
Rat	T	22–24	200	3	5	1.85	5.17	3.85	—	(45)
Rat	V	22–26	160	3	3	1.9	5.5	3.2	—	(86)
Rat	T	15	180	1	5	1.95	5.47	6.5	—	(83)
Rat	T	15	180	1	5	1.95	5.47	6.34	—	(74)
Rat	T	15	200	1	5	1.95	5.39	4.7	11	(46)
Rat	T	22–24	200	3	5	1.95	5.27	3.91	—	(45)
Rat	T	20	200	0.3	3	1.9–2.04	5.26	2.37	—	(77)
Rat	T	23.8	200	1	5	2.0	5.36	—	—	(78)
Rat	T	23.8	200	1	5	2.0	5.36	—	—	(82)
Rat	T	15	200	1	5	2.05	5.43	5.4	9.9	(46)
Rat	T	22–24	200	3	5	2.05	5.36	4.5	—	(45)
Rat	V	RT	160	3	3	2.0–2.1	5.73	3.1	—	(87)
Rat	T	15	180	1	5	2.1	5.5	6	—	(74)
Rat	T	15	180	1	5	2.1	5.51	6.01	—	(83)
Rat	T	20	230	1.5	5	2.1	5.54	5.98	—	(80)
Rat	T	23.8	200	1	5	2.1	5.47	—	—	(82)
Rat	T	23.8	200	1	5	2.1	5.47	—	—	(78)
Rat	T	22	200	1	6.3	2.14	5.6	3.05	—	(66)
Rat	T	15	200	1	5	2.15	5.45	5.6	8.8	(46)
Rat	T	22–24	200	3	5	2.15	5.42	4.54	—	(45)
Rat	V	15	180	—	4.74	2.2	5.51	—	3.2	(71)
Rat	V	15	182	1	5	2.2	5.62	3.1	—	(88)
Rat	V	22	180	1	4	2.2	5.74	2.33	—	(84)
Rat	T	23.8	200	1	5	2.2	5.63	—	—	(82)
Rat	T	23.8	200	1	5	2.2	5.63	—	—	(78)
Rat	T	15	180	1	5	2.25	5.56	5.34	—	(74)
Rat	T	15	200	1	5	2.25	5.49	4.7	7.3	(46)
Rat	T	15	180	1	5	2.25	5.56	5.4	—	(83)
Rat	T	20–22	—	0.5	5	2.2–2.3	6.0	3.75	—	(89)
Rat	T	20–22	—	1.2	5	2.2–2.3	5.65	2.72	—	(89)
Rat	V	22–26	160	3	3	2.3	5.89	4.01	—	(86)
Rat	V	10	200	1	4	2.31	5.36	—	—	(79)
Rat	V	15	200	1	4	2.31	5.68	1.85	3.5	(79)
Rat	V	22	200	1	4	2.31	5.84	—	—	(79)
Rat	T	20	200	0.3	3	2.3–2.5	5.48	2.7	—	(77)
Rat*	T	20–22	—	0.72	—	2.2–2.3	6.2	4.87	—	(89)
Rat*	T	20–22	—	—	—	2.2	6.2	—	—	(95)
Rat*	T	20–22	—	—	—	2.1–2.3	6.19	5.2	—	(2)

T is trabeculae; *V* is ventricle. *RT* is room temperature.
*These preparations were not skinned.

$$[Ca^{2+}]_{50} = [Ca^{2+}]_{50ref}(1 + \beta_1(\lambda - 1)). \quad (12)$$

Backx et al. (2) reported significant differences in Ca^{2+} sensitivity of skinned muscle compared to intact muscle—half-activation is 2–10-fold larger and the Hill coefficient is 2–3 times smaller in skinned muscle. The change in steady-state calcium sensitivity can potentially be rationalized by three different mechanisms:

First, due to intracellular proteins and ions, the spatially averaged Ca^{2+} concentration measured in fluorescence studies does not represent the true concentration of Ca^{2+} in the vicinity of the myofibrils and therefore the concentration of Ca^{2+} at the myofibrils is 2–10 times larger at half-activation (89,90). In this case, the concentration of Ca^{2+} presented to TnC can be scaled by a factor of 2–10, relative to the spatially averaged measures.

Second, the skinning and storage process may reduce the concentration of TnC (91), change the chemical environment (90), or alter the degree of phosphorylation of TnI (92) resulting in a change in the affinity of Ca^{2+} to TnC. This can be represented by increasing the affinity of Ca^{2+} to TnC.

Third, skinning, storage, and a change in chemical environment may cause changes to myosin, actin, tropomyosin, or titin, and the concentration of Ca^{2+} bound to TnC required to cause half-activation may be significantly less in intact preparations and the cooperative mechanisms represented by the Hill coefficient may be degraded (93,94).

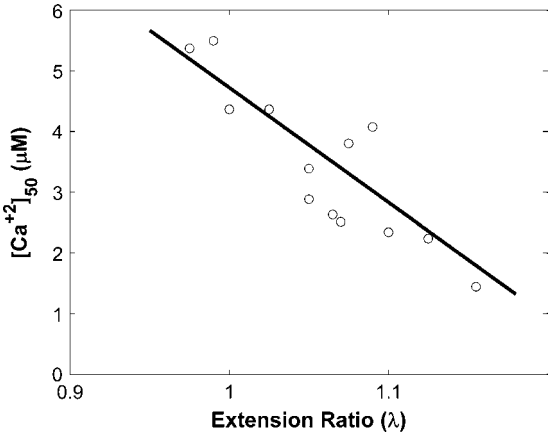

FIGURE 4 Calcium value at half-activation as a function of strain with resting $SL = 2\ \mu$m. (*Solid line*) Points fitted to $[Ca^{2+}]_{50} = 4.72(1–4.0(\lambda-1))$.

Assuming that the affects of skinning on TnC does not alter the capacity of fluorescence data to represent a scalable weighted average of bound Ca^{2+}, free Ca^{2+} in the vicinity of the myofilaments is independent of skinning, assuming the myofilament charge remains unchanged. Then most of the observed changes in Ca^{2+} sensitivity will be a result of the protein–protein interactions after binding of Ca^{2+} to TnC. Hence the affect of skinning can be represented by changing the $[Ca^{2+}]_{50ref}$. Three studies on intact rat preparations with *SL*s of $\approx$2.2 μm calculated the pCa_{50} value to be 6.2 (2,89,95), which compares with a value of $\approx$5.6 for skinned preparations (71,78,82,84,88). $[Ca^{2+}]_{50ref}$ for intact preparations was scaled to account for the variation between intact and skinned preparations, resulting in a $[Ca^{2+}]_{50ref}$ value of 1.05 μM in intact preparations. This definition of $[Ca^{2+}]_{50ref}$ takes into consideration the affects of changes in the chemical environment or degradation of the myofilaments. Insufficient data was available to accurately characterize the length dependence of activation in intact cells, and as a result, β_1 was assumed independent of the skinning process.

Steady-state F-pCa curve

F-pCa curves were defined by $[Ca^{2+}]_{50}$ and the Hill coefficient. The pCa_{50} values defined above at $\lambda = 1.1$ were 5.6 and 6.2 for skinned and intact preparations, respectively. The Hill coefficient has been shown to be both length-dependent (45) and independent (46,73) experimentally. Recent studies by Dobesh et al. (46) showed no length dependence of the Hill coefficient when *SL* was accurately controlled during contraction. Kentish et al. (45) reported a strong length-dependence of the Hill coefficient, but also reported significant sarcomere shortening during contraction, which potentially distorted their results. Here, we assumed that the Hill coefficient is independent of length. A Hill coefficient of 5 was taken from the F-pCa curve for $\lambda = 1.1$ observed by Gao et al. (89), Backx et al. (2), and You et al. (96) for intact rat preparations at room temperature. In skinned preparations, Hill coefficients values range between 1.9 and 10.6. At room temperature, for $\lambda = 1.1$, the Hill coefficient was $\approx$3. It is possible that these curves underestimate the Hill coefficient due to uncontrolled sarcomere shortening as proposed by Dobesh et al. (46), but Dobesh used skinned preparations at 15°C and it is hard to quantify the effect these conditions would have on the Hill coefficients.

The values α_0 and n were found by fitting the steady-state solution of Eq. 9 to F-pCa curves using Eq. 10. The steady-state solution of Eq. 9 was solved iteratively as a function of bound Ca^{2+}. The bound Ca^{2+} was calculated using tension from F-pCa curves defined by half-activation values and Hill coefficients defined above. The resulting values for α_0 and n were 6 s^{-1} and 3.4 and 8 s^{-1} and 3 for skinned and intact preparations, respectively. Fig. 5 shows the fitted F-pCa and idealized F-pCa curves at $\lambda = 1.1$. The dashed and dash-dot lines were calculated from pCa_{50} values 5.6 and 6.2 and Hill coefficients 5 and 3 for skinned and intact preparations, defined above. Solid and dotted lines were generated by the model using the skinned and intact parameter sets.

Maximum activation

In this study, it is assumed that, at maximum activation, not all actin sites are available. However, to ensure that when TnC was saturated the maximum tension reported experimentally was achieved, z was normalized by z_{Max}, such that when $[Ca^{2+}]_{Trpn} = [Ca^{2+}]_{TrpnMax}$,, $z/z_{Max} = 1$ and $T_0 = T_{0Max}$. The value z_{Max} was calculated by solving Eq. 9 with $dz/dt = 0$ and $[Ca^{2+}]_{Trpn} = [Ca^{2+}]_{TrpnMax}$. This is a nonlinear equation and requires an iterative solution method. To maintain an explicit formulation for the model, the nonlinear component was linearized around a point z_p using a Taylor expansion to equal zK_1+K_2, where K_1 and K_2 are

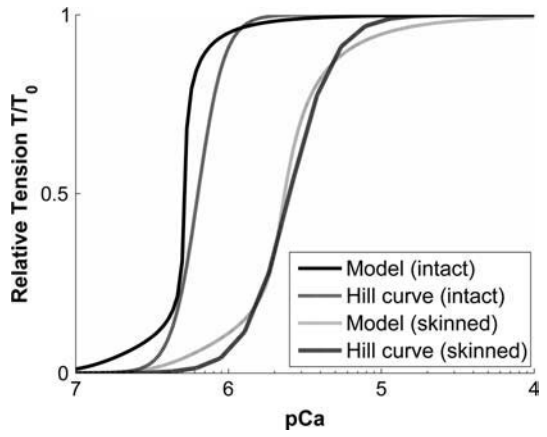

FIGURE 5 Relative steady-state tension with respect to free pCa value. The dashed and dot-dashed lines are calculated from Eq. 10, with pCa_{50} values 5.6 and 6.2 and Hill coefficients 5 and 3 for skinned and intact preparations, respectively, at $\lambda = 1.1$. Solid and dotted lines are generated by the model using the steady-state solution to Eq. 9, with the intact and skinned parameters, respectively.

defined by Eq. 13. The value z_p was set to 0.85 and ensures an error of <1% for $z \in [0.6,1.0]$,

$$K_2 = \alpha_{r2}\frac{z_p^{n_r}}{z_p^{n_r}+K_Z^{n_r}}\left(1-\frac{n_r K_Z^{n_r}}{(z_p^{n_r}+K_Z^{n_r})}\right), \quad K_1 = \frac{\alpha_{r2} z_p^{n_r-1} n_r K_Z^{n_r}}{(z_p^{n_r}+K_Z^{n_r})^2}. \tag{13}$$

The value z_{Max} is then defined by solving the linearized Eq. 9 with $dz/dt = 0$ and $[Ca^{2+}]_{Trpn} = [Ca^{2+}]_{TrpnMax}$, giving

$$z_{Max} = \frac{\frac{\alpha_0}{[Ca^{2+}]^n_{Trpn50}} - K_2}{\alpha_{r1} + K_1 + \frac{\alpha_0}{[Ca^{2+}]^n_{Trpn50}}}. \tag{14}$$

TENSION DEVELOPMENT

Isometric tension

Isometric tension is described in two parts. First, the maximum tension at full activation for a given *SL* (T_{0Max}) is defined using experimentally reported tensions at pCa $\leq$ 4. Secondly, the isometric tension as a function of *SL* and the fraction of available sites is defined by combining $T_0/T_{0Max} = z/z_{max}$ and Eq. 15. The maximum steady-state isometric tension were defined solely by *SL*, as at maximal activation it was assumed that thin filament kinetics would play a minimal role. During *SL* increases, neither crossbridge kinetics (82) or the force generated per bound crossbridge (59) are altered. Gao et al. (89) reported that isometric tension remained the same before and after skinning, whereas interfilament spacing has been shown to increase in skinned cells compared to intact cells (97), indicating that interfilament spacing does not affect the length dependence of isometric tension. The higher maximum tensions at longer *SL* can potentially be explained by an increase in the number of crossbridges that can attach at longer *SL* due to a decrease in the double overlap between actin filaments (76,98–100). The value T_{0Max} is defined by Eq. 15, where λ is equal to *SL* over the resting *SL* of 2 μm (46,101,102), T_{ref} is the maximum tension at resting *SL*, and β_0 is the slope of the $\lambda - T_{0Max}$ relationship,

$$T_{0Max} = T_{ref}(1+\beta_0(\lambda-1)). \tag{15}$$

Limited isometric tension data at varying *SL* values at physiological temperatures was available so the parameters of Eq. 15 were fitted to room temperature results from Table 6. Numerous isometric tension values were reported for varying temperatures, magnesium, and ATP concentrations and preparation types. Fig. 6 plots isometric tensions taken from Table 6 against *SL*. The trend line for isometric tension values recorded under physiological conditions at room temperature (less four outliers) in Fig. 6 was described by Eq. 15 with T_{ref} = 56.2 kPa and β_0 = 4.9, which is close to the β_0 value reported for human myocardium of 4.27 (103). The four excluded results are indicated by the plus, up-triangle, asterisk, and square symbols, three from mouse (*plus-symbol*) (104), cat (*up-triangle*) (105), and guinea pig (*asterisk*) (66), which may indicate a species difference as the favored animal in muscle studies is rat. The remaining anomaly (*square symbol*) (95) is for intact rat muscle but was excluded due to the large standard deviation of 24.1 kPa.

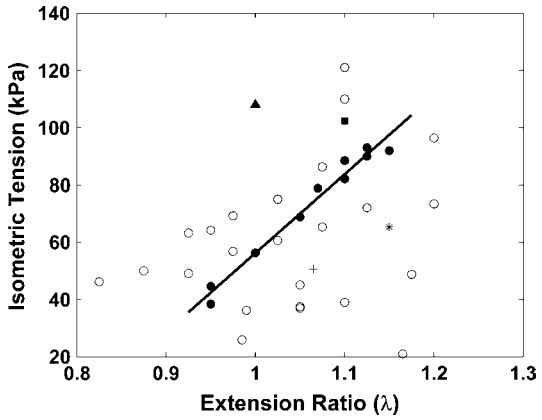

FIGURE 6 Isometric tensions from Table 6 at varying strains, assuming a resting *SL* of 2 μm. Solid data points (46,66,71,72,80,89,104,133) represent measurements taken under physiological conditions defined by $[Mg^{+2}] \approx 0.5$–1 mM (79,89), ATP $\approx$ 4–5 mM, and *SL* is 1.9–2.3 μm (7,73,88) at room temperature 20–22°C. The remaining data from Table 6 is plotted as open circles. Outlying measurements recorded under physiological conditions are marked and correspond to data with large SD. (■) (95) or taken from a species other than rat, namely mouse (+) (104), cat (▲) (105), or guinea pig (*) (66). Line of best fit to solid circles (●) is $T_0 = 56.2(1 + 4.9(\lambda-1))$.

Combing $T_0/T_{0Max} = z/z_{max}$ and Eq. 15 gives Eq. 16, which defines isometric tension as a function of both *SL* and thin filament kinetics,

$$T_0 = T_{0Max}\frac{z}{z_{Max}} = T_{ref}(1+\beta_0(\lambda-1)) \cdot \frac{z}{z_{Max}}, \tag{16}$$

where the value z is the fraction of available actin sites determined by thin filament kinetics and z_{max} is the maximum fraction of available actin sites at a given *SL* as defined above by Eq. 14.

Crossbridge kinetics

The fading memory model (11) provides an efficient method to phenomenologically represent the tension development associated with crossbridge kinetics using a small number of parameters. The fading memory model describes the relationship between tension and sarcomere sliding velocity, by separating tension development into nonlinear static and linear time-dependent components. The linear time-dependent component of the fading memory model is described as the sum of three exponential processes (Eq. 17), where α_i and A_i are the exponential rate constants and associated weighting coefficients; respectively, λ is the strain, $g(T,T_0)$ is a static function of tension and isometric tension, Q_i is the value of the i^{th}

TABLE 6 Isometric tension

Species	Muscle	Prep	Temp (°C)	*SL* (μm)	Mg^{+2} (mM)	ATP (mM)	T_{max} (kPa)	Ref.
Rat	T	SP	23	1.65	3	5	46.2	(45)
Rat	T	SP	23	1.75	3	5	50	(45)
Rat	T	SP	23	1.85	3	5	63.2	(45)
Mouse	P	SP	RT	1.9	1	5	38.4	(104)
Rat	T	SP	20	1.9	1	4	44.6	(72)
Rats	V	SP	15	1.95	1	5	56.8	(46)
Rat	T	SP	23	1.95	3	5	69.2	(45)
Rat	V	SP	20	1.98	3	3–5	36.25	(77)
Cat	T	IP	25	2.0	—	—	108	(105)
Rat	T	SP	20	2	1	4	56.3	(72)
Rats	V	SP	15	2.05	1	5	60.6	(46)
Rat	T	SP	23	2.05	3	5	75	(45)
Rat	T	SP	20	2.1	1	4	68.8	(72)
Rat	T	SP	20	2.1	1.5	5	37	(80)
Rat	T	SP	20	2.1	3	5	37.5	(128)
GP	T	SP	22	2.13	1	6.3	50.6	(66)
Rat	T	SP	22	2.14	1	6.3	78.9	(66)
Rat	T	SP	23	2.15	3	5	86.3	(45)
Rats	V	SP	15	2.15	1	5	65.3	(46)
Rat*	T	IP	22	2.2	—	—	88.5	(133)
Rat†	T	IP	22	2.07–2.2	—	—	45.1	(133)
Rat	V	SP	15	2.2	1	5	39	(88)
Rat	T	SP	20	2.2	1	4	82.1	(72)
Rat	T	IP	20–22	2.2	—	—	102.4	(95)
Rat	T	IP	20–22	2.1–2.3	1.2	5	121	(2)
Rat	T	SP	20	2.2–2.3	0.5	5	90	(89)
Rat	T	IP	20	2.2–2.3	0.72	—	93	(89)
Rats	V	SP	15	2.25	1	5	72	(46)
Rat	V	SP	20	2.35	3	3–5	48.8	(77)
Rat	T	SP	20	2.3	1	4	92.0	(72)
Mouse	P	SP	RT	2.3	1	5	65.3	(104)
Rats	V	SP	13	2.29–2.36	1	4	21	(110)
Rat	T	SP	20	2.4	1	4	96.4	(72)
Cat	V	IP	30	—	—	—	18	(55)
Ferret	P	IP	30	—	—	—	54.4	(57)

SL is sarcomere length. *GP* is guinea pig; *P* is papillary; *T* is trabeculae; *V* is ventricle. *IP* is intact preparation. *RT* is room temperature. *SP* is skinned preparation.
*Controlled *SL*.
†Uncontrolled *SL*.

integral, and n is the number of exponential processes. Cell models are commonly defined in terms of a system of ordinary differential equations. To adapt the fading memory model to fit this mold, the right-hand side of Eq. 17 was differentiated by time to give Eq. 18,

$$g(T,T_0)=\sum_{i=1}^{n}A_i\int_{-\infty}^{t}e^{-\alpha_i(t-\tau)}\frac{d\lambda}{dt}d\tau=\sum_{i=1}^{n}Q_i,$$

where

$$Q_i=Q_i=A_i\int_{-\infty}^{t}e^{-\alpha_i(t-\tau)}\frac{d\lambda}{dt}d\tau \tag{17}$$

$$\frac{dQ_i}{dt}=A_i\frac{d\lambda}{dt}-\alpha_iQ_i. \tag{18}$$

Under conditions of steady-state shortening, Eq. 17 yields the well-known Hill force-velocity relation if g in Eq. 17 is chosen to be $g(T/T_0)=(1-T/T_0)/(T/T_0+a)$. Choosing g as a single function of T/T_0 is also consistent with the idea that the force scales with the number of active crossbridges, reflected in T_0. Hill's force-velocity curve describes the shortening (positive velocities) but not the lengthening (negative velocities) of the muscle under a constant load. The velocity becomes negative when the constant load is greater than the isometric tension ($T > T_0$). Here, the Hill curve was extended to model negative velocities. In frog skeletal muscle at 0°C, the magnitude of the negative velocity increases significantly for $T > 1.4\ T_0$, but no information was available for more negative velocities or larger tensions in cardiac muscle (100). It was assumed that the force v's velocity relationship for negative velocities was a reflection of the plot for positive velocities. The original Hill curve for positive velocities is equal to Eq. 19 for $V > 0$ and the extended curve for negative velocities is equal to Eq. 19 for $V < 0$. In Eq. 19, V is the sarcomere velocity, V_0 is the maximum velocity, T is the active tension, T_0 is the isometric tension, and a is a measure

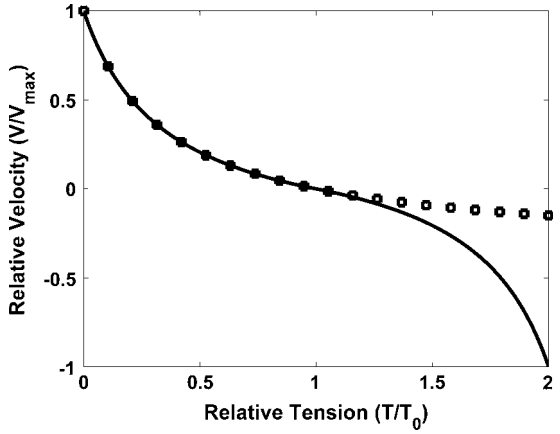

FIGURE 7 The □ data points are calculated from the original Hill equation with $a = 0.35$. The solid line indicates adapted Hill equation for $T/T_0 > 1$.

of the curvature of the force-velocity relation (the value a is equivalent to aT_0 in Hill's original equation). The original and extended Hill curves are depicted in Fig. 7. The resulting force-velocity relationship is C_1 (slope) continuous, which provides numerical stability for the computational solution method as described later.

$$-V\frac{1}{aV_0} = \begin{cases} \dfrac{T/T_0 - 1}{T/T_0 + a} & V > 0 \\ \dfrac{T/T_0 - 1}{2 + a - T/T_0} & V < 0 \end{cases}. \qquad (19)$$

Experimental results from constant velocity experiments in cardiac muscle give values of a as 0.2 (106), 0.5 (1), 0.35 (107), and 0.25 (108). The value a is also dependent on the exercise regime ($a \approx 0.2$–0.36) (109) and P_i concentration ($a \approx 0.32$–0.36) (110). Considering these values, a was set to 0.35. Other authors have reported values for a ranging from 0.05 (111) to 0.8 (112) by fitting limited regions of the force-velocity curve. It has been noted that the Hill equation does not fit the force-velocity curve for small velocities (111–113), but the approximation error is relatively small.

During constant velocity experiments $d\lambda/dt = -V$, and the linear component of the fading memory model (right-hand side of Eq. 17) is equal to

$$\sum_{i=1}^{n} Q_i = -V \sum_{i=1}^{n} \frac{A_i}{\alpha_i}. \qquad (20)$$

Setting the sum of $A_i/\alpha_i = 1/(aV_0)$ means that the sum of Q_i in Eq. 17 is equal to the right-hand side of Eq. 19. This forms the relationship between the linear time-dependent and nonlinear static components of the fading memory model. The final form of the fading memory model was described by Eq. 21. The extended Hill equation proposed in Eq. 19 ensures that the denominator of Eq. 21 is always greater than or equal to one, thereby removing the singularity that would be present if the standard Hill equation were used for both positive and negative velocities.

$$T = \begin{cases} T_0 \dfrac{a\sum_{i=1}^{n} Q_i + 1}{1 - \sum_{i=1}^{n} Q_i} & \sum_{i=1}^{n} Q_i < 0 \\ T_0 \dfrac{1 + (2+a)\sum_{i=1}^{n} Q_i}{1 + \sum_{i=1}^{n} Q_i} & \sum_{i=1}^{n} Q_i > 0 \end{cases}. \qquad (21)$$

The linear time-dependent component of the fading memory was described by three exponential processes (11,114) and requires the definition of three rate constants and three amplitude coefficients. Although the effect of temperature on crossbridge kinetics is significant, there was insufficient data to characterize crossbridge kinetics at physiological temperatures and, as such, the parameter set defined here will be for room temperature, where room temperature was taken as 20–23°C. Sinusoidal analysis provides two rate constants explicitly. The four remaining parameters were fitted using the two defined rate constants and four constraints derived from experimental results. These constraints are outlined in detail in the following sections. First, sinusoidal analysis was used to find the minimum stiffness frequency, maximum phase shift frequency, and the high frequency stiffness. Secondly, the instantaneous step change required to drop tension to zero was determined, which required the high frequency stiffness values from the sinusoidal analysis. Thirdly, the maximum velocity was defined. The remaining four fading memory model parameters were then fitted using the four constraints and the two defined rate constants.

Dynamic stiffness

Sinusoidal analysis provides two of the rate constants explicitly and the minimum dynamic stiffness frequency, the maximum phase shift frequency, and the high frequency stiffness are used to constrain the remaining parameters. The dynamic stiffness of muscle has been effectively measured by imposing a small sinusoidal or random noise perturbation while the muscle is in isometric contraction. The dynamic stiffness is equal to the tension over the applied length change and can be described in the frequency domain using Eq. 22 as proposed by Kawai and Brandt (115) or in the time domain using the fading memory model (Eq. 17). In Eq. 22, $a < b < c < d$ are the rate constants and are equal to the corresponding α_i values from Eq. 17 over 2π. A, B, C, and D are coefficients and equal to the product of the corresponding A_i values in Eq. 17 and $T_{ref}(1+a)$. Using standard nomenclature, the negative coefficient is B. In cardiac muscle, B has the lowest rate and no A process is seen. H is the linear

passive stiffness, which was not considered in the model of active contraction described here:

$$E = H + A\frac{if}{if + a} + B\frac{if}{if + b} + C\frac{if}{if + c} + D\frac{if}{if + d}. \quad (22)$$

Rossmanith et al. (116) showed that the myosin isoform present in the preparation played a prominent role in determining crossbridge kinetics and results from sinusoidal analysis. Ventricular myosin in mammals appears in three different forms—i.e., V_1, V_2, and V_3. The predominant forms are V_1 and V_3 or α and β, respectively, and their presence is determined by species and thyroid state. In ferret and rabbit, V_1 is commonly expressed whereas in bovine, humans, and rats, the V_3 type is predominant (116,117). Considering this, crossbridge kinetic results will be taken preferentially from rat, human, and bovine preparations.

Sinusoidal perturbation experiments are commonly performed in skinned preparations at full activation (pCa < 4) and $\lambda > 1.1$. At full activation, $[Ca^{+2}]_{Trpn}/[Ca^{+2}]_{TrpnMax} \approx 1$ and $z/z_{Max} \approx 1$, such that dynamic stiffness (E) is equal to (11):

$$E|_{pCa<4} = T_0\left(\beta_0 + (1 + a)\sum_{k=1}^{3} A_k\frac{if}{if + \frac{\alpha_k}{2\pi}}\right). \quad (23)$$

Measurements of coefficients and rate constants from sinusoidal perturbation experiments are presented in Table 7. Experiments by Kawai et al. (118), Saeki et al. (114), and Shibata et al. (119,120) in ferret and rabbit preparations recorded similar results for V_1 myosin isoforms. Results by Wannenburg et al. (82) in rat myocardium are considerably different. However, Wannenburg et al. (82) did not report rates or coefficients with process D fitted, although they commented that the exclusion of process D had minimal affect on the rates of processes B and C (α_1 and α_2). The converted rate constants b and c (i.e., $\alpha_1 = 30.78\ s^{-1}$ and $\alpha_2 = 132.6\ s^{-1}$) reported by Wannenburg et al. (82) are comparable to measurements by Ruf et al. (121) and Campbell et al. (122) for human and rat myocardium, respectively, and will be used in the model.

Dynamic stiffness data is commonly represented in two plots—the dynamic modulus plot of the absolute value of dynamic stiffness against frequency, and the phase shift against frequency plot. The Nyquist diagram plots phase against amplitude. The dynamic modulus plot exhibits a characteristic dip in stiffness at the minimum stiffness frequency (f_{min}). The phase shift plot has a single maximum at the maximum phase shift frequency (Θ_{max}) (115). These two frequencies provide two points of reference and ensure that the model produces characteristic plots. Table 8 lists reported f_{min} and Θ_{max} values. The value f_{min} was calculated using a range of species and temperatures. The value f_{min} increases significantly with temperature from 1 Hz to 17.25 Hz at 20°C and 40°C, respectively. There was no definitive relationship between myosin isoform and f_{min}. Rabbit and ferret have reported f_{min} values of 0.9–2 Hz at room temperature. However, the 2 Hz result was recorded with ATP at 1 mM; excluding this value reduces the range to 0.9–1.44 Hz. Rat and bovine f_{min} values range between 1 and 3.2 Hz. The 3.2 Hz reported by Wannenburg et al. (82) was for partially activated preparations, but Wannenburg et al. (82) did note that this had a minimal affect on f_{min}. Rossmanith et al. (116) reported that V_1 and V_3 myosin isoforms had an f_{min} value of 1.2 Hz and 2.2 Hz, respectively, at 25°C. The value f_{min} for the model was taken to be 2 Hz. The value Θ_{max} was reported less often than f_{min}, and ranges between 2.1 and 8 Hz. It was not known how partial activation affects Θ_{max}, so the Wannenburg et al. (82) results are not considered here. The value Θ_{max} for human data is 4.3 Hz (123), which is comparable to rat (4 Hz) (116), rabbit (4 Hz) (119,124), and ferret (3.5 Hz) (118) myocardium. Considering these results, the Θ_{max} for the model was taken as 4 Hz.

The high-frequency stiffness (HFS) is the stiffness calculated using the model at pCa < 4 and $f \to \infty$ (Eq. 24). Experimentally, the HFS is the stiffness at the highest frequency recorded:

$$E|_{f=\infty} = T_{ref}\beta_0 + T_{ref}(1 + a)\sum_{k=1}^{n} A_k. \quad (24)$$

The HFS varies significantly between authors. Campbell et al. (122) measured HFS of ≈0.2–1 M Nm^{-2} at varying isometric tensions using a low maximum frequency range

TABLE 7 Sinusoidal analysis results

Species	Temp (°C)	pCa	Frequency range (Hz)	B	$2\pi b$	C	$2\pi c$	D	$2\pi d$	Ref.
Ferret*	20	Ba^{2+}†	0.13–135	0.82	7.6	2.09	26	0.90	682	(114)
Ferret	20	4.55	0.13–135	0.72	8.6	1.57	30	0.59	703	(114)
Ferret	20	4.82	0.13–135	0.58	9.9	1.31	23.6	0.42	552	(118)
Rat	23	6.11	0.5–70	1.09	5.97	3.49	47	—	—	(82)
Rat	23	5.92	0.5–70	2.92	30.78	11.3	133	—	—	(82)
Human‡	35	5	0.125–100	0.376	25	0.525	70.37	—	—	(123)
Rat	—	4.3	0.1–40	—	33.6	—	190.4	—	—	(122)
Ferret	—	—	0.1–40	—	30.41	—	70.56	—	—	(122)

*These preparations were not skinned.
†Barium contractures.
‡Human patients on numerous medications before the preparations were sampled; patients had an average age of 61.2 years.

TABLE 8 Maximum phase shift and minimum dynamic stiffness

Species	Temp (°C)	Θ_{max} (Hz)	F_{min} (Hz)	Comments	Ref.
Human	35	4.3	9		(123)
Bovine	40	—	17.25		(127)
Bovine	30	—	5.21		(127)
Bovine	20	—	1		(127)
Bovine	25	7.6	2	5 mM ATP	(151)
Rat	25	4	1.8		(116)
Rat	23	8	3.2	pCa 5.92	(82)
Rabbit	24	4.0	1.2		(119)
Rabbit	24	4	1.44		(124)
Ferret	20.2	2.1	1.3	Skinned	(114)
Ferret	20.2	1.7	0.9	Intact	(114)
Ferret	20	3	2	1 mM ATP	(118)
Ferret	20	3.5	2	1 mM ATP	(118)

(40 Hz). Wannenburg et al. (82) reported the HFS to be $\approx$7.25 M Nm^{-2}, again using a low maximum frequency (70 Hz). The experiments were performed at only partial activation but recorded viable isometric tensions (87 kPa) at full activation. Kawai et al. (118) recorded HFS values of $\approx$0.9 M Nm^{-2} using a maximum frequency of 135 Hz, but measured low isometric tension values (18.3 kPa) and inorganic phosphate concentrations were high (8 mM) in skinned preparations. Mulieri et al. (123) recorded an HFS of $\approx$0.59 M Nm^{-2} in human hearts of patients (average age 61.6) at a maximum frequency of 100 Hz. Saeki et al. (114) recorded HFS values of 2.50 and 1.44 M Nm^{-2} for intact and skinned preparations, respectively, using a maximum frequency of 135 Hz, but recorded isometric tensions of 49 kPa and 26 kPa for intact and skinned preparations, respectively, at L_{max} ($SL \approx 2.3$ μm). The isometric tension values recorded at full activation in sinusoidal analysis experiments were characteristically low when compared with static isometric tension data from Table 6. The large variations in HFS values meant that these data were not used directly to fit model parameters but instead were used in the following section to define the length step required to drop tension to zero.

Length-step experiments

The step response of the fading memory model is found by setting $\lambda(t) = \Delta\lambda \times H(t)$, where $H(t)$ is the Heaviside step function, or equivalently $d\lambda/dt = \Delta\lambda \times \delta(t)$, where $\delta(t)$ is the Dirac δ-function (11). This gives

$$\frac{T/T_0 - 1}{T/T_0 + a} = \Delta\lambda \sum_{i=1}^{n} A_i e^{-\alpha_i t}. \quad (25)$$

The length step required to drop tension to zero immediately after a length change is found by setting $t = 0$ in Eq. 25 and is equal to Eq. 26:

$$\frac{-1}{a\sum_{i=1}^{n} A_i} = \Delta\lambda. \quad (26)$$

Instantaneous length steps are not possible in real experiments due to the inertia of testing equipment and muscle. To overcome this, various experimental methods have been proposed to elucidate the magnitude of $\Delta\lambda$. The value T_1 is the tension after a rapid length step over a finite duration of time. For length steps over a finite duration of time (Δt) with $T_1 = 0$, there is a linear relationship between $\Delta\lambda$ and Δt (100). Hunter et al. (11) exploited this relationship to determine $\Delta\lambda$ of 0.5%, as Δt tends to zero using frog and ferret data (at 0°C and 27°C, respectively). Backx and ter Keurs (125) used a similar method to determine a $\Delta\lambda$ value of 1.2% in rat muscle (at 5°C). An alternate method is to assume a linear relationship between tension and small length changes, such that $\Delta\lambda$ is equal to the ratio of the high frequency stiffness (HFS) and isometric tension. The HFS value is not used in isolation, as it varies considerably between authors as mentioned above. However, the ratio of HFS to isometric tension varies less and appears to be less sensitive to myosin isoform, temperature, and muscle viability than HFS alone. At an SL of 2.1 μm, Wannenburg et al. (82) measured the ratio of HFS to maximum isometric tension as 1.2%, which is comparable to HFS measurements at L_{max} (the muscle length, which achieves maximum tension or $SL \approx 2.3$ μm) of 1.6–2.0% by Shibata et al. (120), Saeki et al. (114), and Kawai et al. (118). Considering the results of both modalities, the value of $\Delta\lambda$ required to drop tension to zero in this model will be set to 1.2%.

Maximum velocity experiments

The maximum velocity (V_0) of contraction is directly related to ATPase (111,126), and as such, indicative of crossbridge kinetics. The maximum velocity occurs under zero load, and is independent of SL for SL values between 1.9 and 2.2 μm (111). The fading memory model parameters can be constrained using Eq. 27 and results from maximum velocity experiments (11),

$$\frac{1}{aV_0} = \sum_{i=1}^{n} \frac{A_i}{\alpha_i}. \quad (27)$$

Maximum velocity experiments are performed over a range of temperatures as reported in Table 9, but can be adjusted to

TABLE 9 Maximum muscle velocity at 23°C; strain rates adjusted to 23°C using a Q_{10} value of 4.6

Species	Original temp (°C)	Strain rate (s^{-1})	Strain rate at 23°C (s^{-1})	Ref.
Rat	25	13.3	9.8	(149)
Rat	20	6.13	9.6	(111)
Rat	25	12.68	9.34	(111)
Rat	30	23.44	8	(111)
Rat	12	3.45*	18.5	(150)
Cat	25	9.8	7.2	(105)
Rat	22	9.82*	11.4	(84)

*Calculated using ML s^{-1} and SL.

room temperature using a Q_{10} of 4.6 (111). A maximum velocity per sarcomere of $\approx$19 μm s^{-1} or a strain rate of 9.5 s^{-1} at room temperature with a resting *SL* of 2 μm was set to constrain the parameters in Eq. 23.

Fading memory model parameters

The linear time-dependent component of the fading memory model has three rate (α_i) values and three coefficient (A_i) values. The frequency values of $\alpha_1 = 30$ s^{-1} and $\alpha_2 = 130$ s^{-1} were set directly to those reported by Wannenburg et al. (82), as explained above. The remaining four parameters were calculated by determining the best fit to the four independent constraints outlined above. These are, the maximum velocity (Eq. 27), length step experiments (Eq. 26), and f_{min} (2 Hz) and Θ_{max} (4 Hz) frequencies. The fitting process was begun by setting A_1 and A_2, then calculating A_3 using Eq. 26, then α_3 was determined using Eq. 27 and finished using Eq. 23 to determine f_{min} and Θ_{max} numerically. Thus, by searching the parameter space of A_1 and A_2, the best parameter set for the four constraints was determined. The resulting values for the process magnitudes A_1, A_2, and A_3 are -29, 138, and 129, respectively. The process rates α_1, α_2, and α_3 are 30 s^{-1}, 130 s^{-1}, and 625 s^{-1}, respectively. The resulting f_{min} and Θ_{max} values are 0.9 Hz and 3.75 Hz, respectively. The value f_{min} was smaller than the f_{min} value determined above, from V_3 myosin experimental results; however, it was still comparable with V_3 myosin results from Fujita and Kawai (127) (f_{min} = 1 Hz) and V_1 myosin results.

MODEL SUMMARY

The complete model is summarized, with the set of parameters for (primarily intact rat ventricular) cardiac muscle at room temperature. The model can be adapted to represent skinned preparations by changing α_0, n, and $[Ca^{2+}]_{50ref}$ to 6 s^{-1}, 3.4, and 4.72 μM, respectively.

Parameters

TnC-Ca binding

Equations 2 and 3, where $k_{on} = 100$ μM^{-1} s^{-1}; $k_{offref} = 200$ s^{-1}; $\gamma = 2.0$; and $[Ca^{2+}]_{TrpnMax} = 70$ μM.

Tropomyosin kinetics

Equations 9, 11, and 14, where $\alpha_{r1} = 2$ s^{-1}; $\alpha_{r2} = 1.75$ s^{-1}; $K_z = 0.15$; $n_r = 3$; $\beta_1 = -4.0$; $\alpha_0 = 8$ s^{-1}; $n = 3$; $z_p = 0.85$; and $[Ca^{2+}]_{50ref} = 1.05$ μM.

Tension development

Equations 15, 18, and 21, where $T_{ref} = 56.2$; $\beta_0 = 4.9$; $a = 0.35$; $A_1 = -29$; $A_2 = 138$; $A_3 = 129$; $\alpha_1 = 30$ s^{-1}; $\alpha_2 = 130$ s^{-1}; and $\alpha_3 = 625$ s^{-1}.

VALIDATION

The three model components, Ca^{2+} binding to TnC kinetics, tropomyosin kinetics, and crossbridge kinetics, have been constructed and parameterized in isolation using a wide range of preparation types and spatial scales. Comparison has already been made with experimental data isolating the function of each component from data using the parameter set allocated in previous sections. To validate tropomyosin kinetics, model simulations were compared with caged Ca^{2+} experiments. Crossbridge kinetics were validated using tension transients after rapid length increases. No obvious experimental results were available to validate Ca^{2+} binding to TnC kinetics, but the functional form of Ca^{2+} binding to TnC (Eq. 2) is a generally accepted model and the tension dependence of the unbinding rate can be derived from length-step experiments (Eqs. 4–8). To ensure that when the ensemble of model components were integrated together the resulting simulations matched experimental results, model simulations were compared with *SL* clamped and *SL* unclamped tension traces. Finally, to test that the complete model was able to characterize RT_{50}, a comparison was made between simulated RT_{50} and experimental measurements at increasing muscle length.

Caged calcium activation curves

To verify tropomyosin kinetics, which were defined by tension relaxation and F-pCa curves, the model was compared with caged calcium release experiment results. In caged Ca^{2+} experiments nitrophenyl-EGTA is saturated with Ca^{2+} and then exposed to a flash of light resulting in a rapid decrease in the Ca^{2+} affinity, causing a rapid increase in the concentration of free Ca^{2+} (60). This provides a means of measuring the rate of tension development after a step change in Ca^{2+}. Tropomyosin activation kinetics were defined using the relaxation kinetics and F-pCa curves. Fig. 8 plots tension traces for guinea-pig caged Ca^{2+} experiments with $SL = 2.18$ μm at 23°C, taken from Martin et al. (81) against simulated results using the skinned preparation parameter set. The Ca^{2+} concentrations after the release of caged Ca^{2+} was calculated using the final relative tensions and F-pCa curves for skinned preparations described above with $pCa_{50} = 5.6$ and $n = 3$.

Finite duration length-step changes

For a 1-ms length step of 1% ($SL = 2.1$ μm) at room temperature at an inorganic phosphate concentration of 0 mM, the half-relaxation time is 6.0 ms (128), compared with a half-relaxation time of 6.2 ms predicted by the model (see Fig. 9). The model also exhibits the characteristic dip seen when muscle is rapidly stretched, but shows no evidence of further oscillations observed by Saeki et al. (129) and Berman et al. (124). The fading memory model

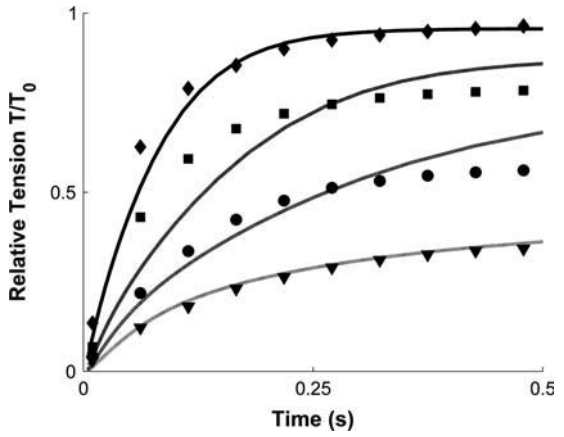

FIGURE 8 Tension transients after the release of caged Ca^{2+} by nitrophenyl-EGTA with $SL = 2.18$ μm and initial pCa = 7. Data points are from Martin et al. (81) and lines are from model simulations. The ▼ data points and dashed line, ● data points and dash-dot line, ■ data points and dotted line, and ♦ data points and solid line had pCa values after the release of the caged calcium of 5.07, 5.41, 5.56, and 5.69, respectively. The pCa values were calculated using the final relative tensions and the skinned F-pCa curve defined below with a Hill coefficient of $n = 3$ and half-activation value of $pCa_{50} = 5.6$.

predicts a significant rise in tension after a rapid length decrease, analogous to the dip in rapid length increase experiments. The rise predicted by the model after the length decrease was not seen in rapid length decrease experiments in cardiac muscle performed by Hancock et al. (130), but has been observed in both skeletal muscle (131) and cardiac muscle (132) for very small step sizes ($\Delta\lambda \leq 0.5\%$).

Clamped and unclamped sarcomere length isometric twitches

Inhomogeneous *SL* shortening in muscle preparations during an isometric twitch has been shown to cause a significant decrease in developed tension. Janssen and de Tombe (133) showed that using iterative feedback *SL* control, the *SL* could be held constant, resulting in significantly increased developed tension and a decrease in the amplitude of the $[Ca^{2+}]_i$ transient. The tension traces for clamped and unclamped experiments recorded by Janssen et al. (7) were simulated by the model using the corresponding experimental $[Ca^{2+}]_i$ and *SL* traces. The fluorescent traces from Janssen and de Tombe were converted to $[Ca^{2+}]_i$ values using $[Ca^{2+}]_i = K'_d(R-R_{min})/(R_{max}-R)$, where $K_d' = 2.95$ μM, $R_{max} = 10$, $R_{min} = 0.2$, and R is the fluorescence ratio. K_d' and R_{max} are taken from Gao et al. (3,89) and R_{min} is set such that resting $[Ca^{2+}]_i$ is ≈0.1 μM. The calculated $[Ca^{2+}]_i$ transient and the experimentally measured *SL*s are shown in Fig. 10 *A*. Cubic splines were fit through the data to produce smooth curves to input into the model and to compare with simulation results. The resulting simulated tension traces are compared with experimental measurements in Fig. 10, *B* and *C*. The simulated results are similar to experimental measurements, al-

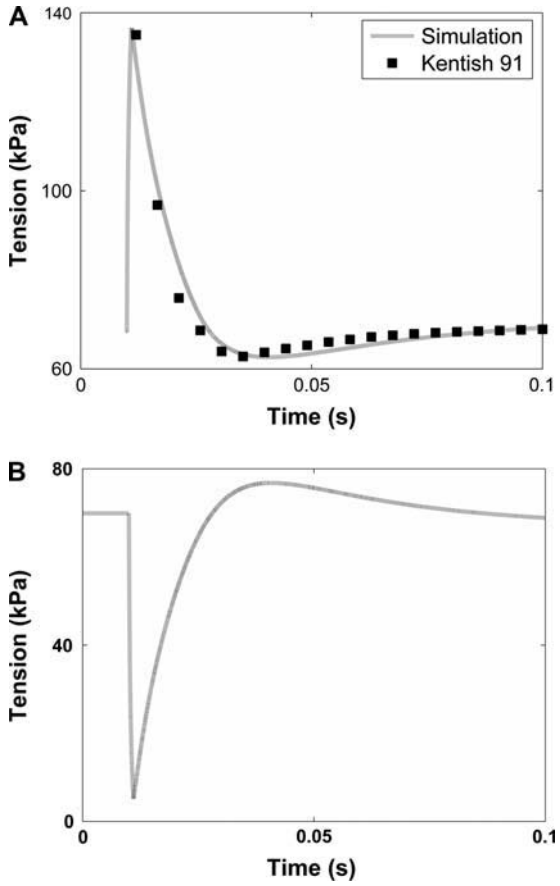

FIGURE 9 Length steps of 1-ms duration. (*A*) 1% length-step increase at 23°C for $SL = 2.1$ μm and pCa = 4. The dashed line is the model prediction; ■ is from Kentish (128), (tension scaled to model). (*B*) 1% length-step decrease at 23°C, for $SL = 2.1$ μm and pCa = 4.

though the final stages in the unclamped simulations were notably slower and slightly slower in the clamped simulations. However, RT_{50} values were well represented by the model.

Half-relaxation times

As cardiac muscle is stretched at room temperature RT_{50} during isometric twitch increases (7). Fig. 11 *B* compares RT_{50} for intact rat trabeculae at 22.5°C from Janssen et al. (7) with simulation results from the model. Results from Janssen and others were recorded at 10 equally spaced lengths between the resting length and maximum tension length, which are assumed to correspond to equally spaced *SL* values between 1.8 μm and 2.2 μm for simulations. The *SL* was assumed to remain constant during the isometric twitch, although *SL* was not controlled by feedback iterations in the study of Janssen et al. (7). Thus the $[Ca^{2+}]_i$ transient is held fixed for all simulations. Tension transients at each muscle length are shown in Fig. 11 *B*. The $[Ca^{2+}]_i$ transient is expected to vary at differing *SL*s, but limited experimental data is available to characterize this phenomenon.

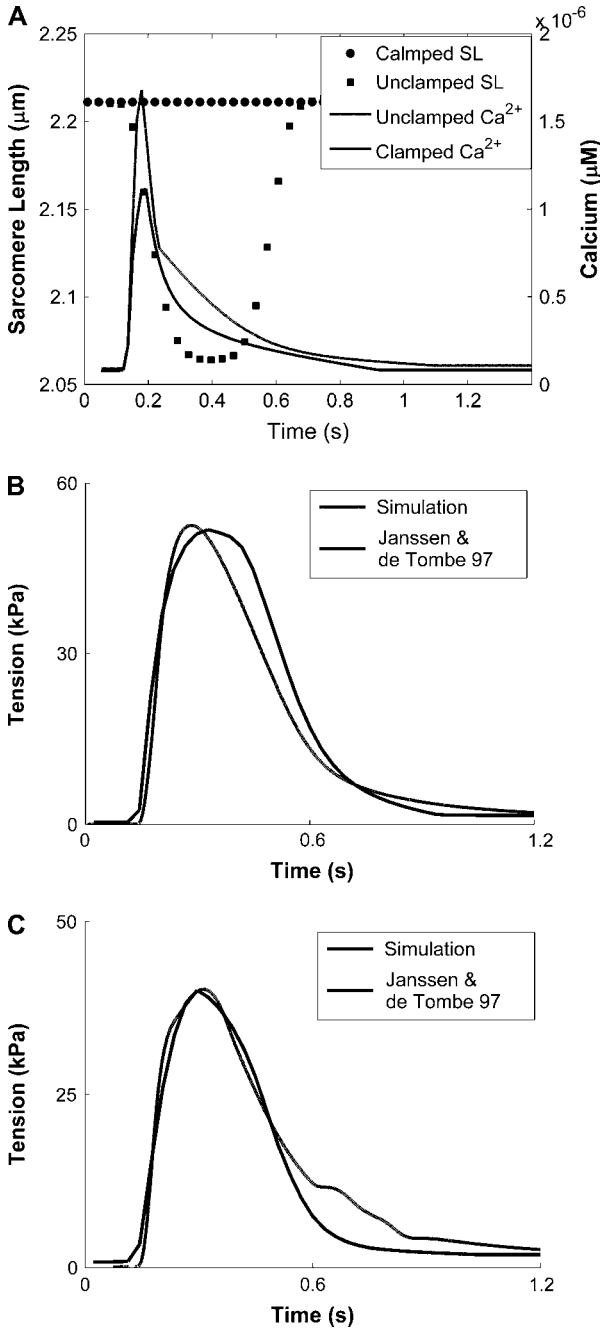

FIGURE 10 (*A*) Sarcomere lengths from unclamped *SL* (■) and clamped *SL* (●) experiments from Janssen and de Tombe (133). $[Ca^{2+}]_i$ transients from unclamped *SL* (*dashed line*) and clamped *SL* (*solid line*) experiments. $[Ca^{2+}]_i$ transients were calculated from fluorescence data from Janssen and de Tombe (133) and converted to $[Ca^{2+}]_i$ values using $[Ca^{2+}]_i = K'_d(R-R_{min})/(R_{max}-R)$, where $K'_d = 2.95$ μM, $R_{max} = 10$, $R_{min} = 0.2$ (4,89). (*B* and *C*) Clamped and unclamped experiments, respectively; experimental data are taken from Janssen and de Tombe (133) (*solid lines*), and lines are generated by the model (*dashed lines*).

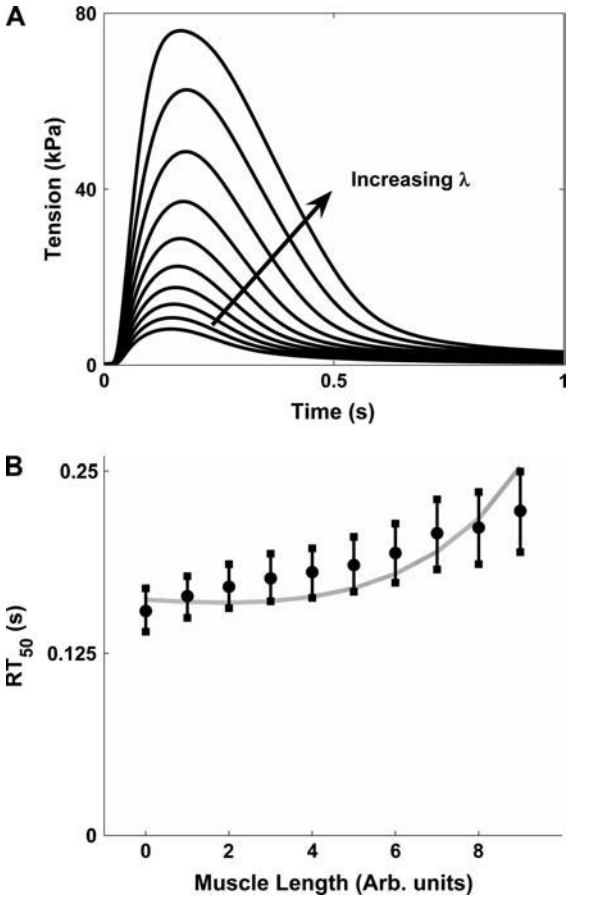

FIGURE 11 (*A*) Tension traces for increasing *SL* from 1.8 μm to 2.2 μm. (*B*) RT_{50}, points taken from Janssen et al. (7) at room temperature, with standard error. Line calculated from model simulations. Arbitrary units defined by Janssen et al. (7).

RELAXATION FACTORIAL ANALYSIS

The $[Ca^{2+}]_i$ transient, TnC kinetics, and length dependence have all being implicated in determining RT_{50} (134). It is worth noting that many of the factors are coupled, via tension dependence, which often results in inconclusive experimental findings. To determine the relative importance of the factors listed in Table 10 on RT_{50}, a full factorial analysis (135) was performed. A factorial analysis provides a means to analyze the relative importance of a single factor and multiple factor interactions on a given output, by approximating the output as a linear function of all the factors and determining the coefficients. The magnitude of the coefficients indicates the relative influence of each factor, including multiple factor interactions. Although factorial analysis uses a linear approximation of a nonlinear output, which is not ideal, it provides a feasible means to identify significant factors, which can then be analyzed in detail. The output was defined as the RT_{50} value for an isometric twitch with a prescribed $[Ca^{2+}]_i$ transient and clamped $SL = 2.2$ μm. Table 10 summarizes the factor definitions and values, and

TABLE 10 Factors and variable descriptions and values for factorial experiment

Factor #	Variable	High value (+)	Low value (−)
1	Unbinding rate of Ca^{2+} from TnC	$k_{off} = 220\ s^{-1}$	$k_{off} = 180\ s^{-1}$
2	Length-dependent sensitivity	$\beta_0 = 5.4$	$\beta_0 = 4.41$
3	Length-dependent maximum tension	$\beta_1 = -1.3$	$\beta_1 = -1.06$
4	$[Ca^{2+}]_i$ transient magnitude	110%	90%
5	Tension-dependent binding of Ca^{2+} to TnC	$\gamma = 2.2$	$\gamma = 1.8$

Fig. 12 *A* shows the relative influences. During the factorial analysis, the β_0- and γ-values used to calculate the concentration of calcium bound at half-activation (Eq. 11) were held constant, since they do not represent any mechanism in this equation. The factorial analysis identified the $[Ca^{2+}]_i$ transient magnitude and the unbinding rate of Ca^{2+} from TnC as the two most significant factors within the initial parameter space. A detailed analysis of the parameter space of the unbinding of Ca^{2+} from TnC and the magnitude of the $[Ca^{2+}]_i$ transient on RT_{50} is shown in Fig. 12 *B* to illustrate coupled effects and to determine whether the effect of each factor is dependent on the parameter space.

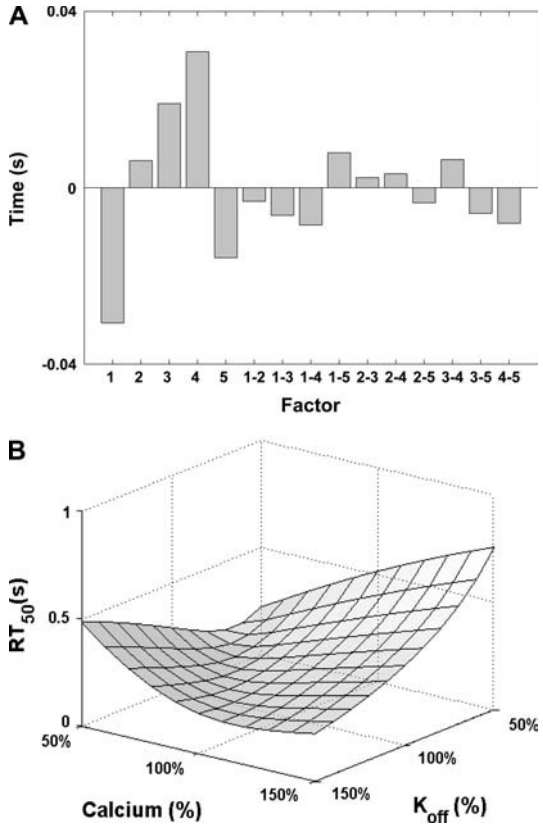

FIGURE 12 (*A*) Relative effects of individual and two-factor interactions for prescribed $[Ca^{2+}]_i$ transient and $SL = 2.2\ \mu m$. Single-digit factors correspond to the variables listed in Table 10 and two-digit factors indicate the coupled effect of the variables from Table 10 corresponding to each digit; for example, 45 corresponds to the coupled affect of the $[Ca^{2+}]_i$ transient and the tension dependence of Ca^{2+} binding to TnC . (*B*) The RT_{50} calculated using the model with the $[Ca^{2+}]_i$ and the unbinding rate of Ca^{2+} from TnC varying between 50 and 150% of their original values.

DISCUSSION

In this article, we present an improved version of the HMT model for the active contraction of cardiac muscle and analyze its behavior, particularly during relaxation. Each model parameter was determined from a broad range of experimental results. The model components and the coupling between them were subsequently validated against a wide range of experimental protocols. After development and validation, the model was used to quantify the relative influence of the tension-dependent unbinding rate of Ca^{2+} from TnC, length-dependent sensitivity, length-dependent maximum tension, $[Ca^{2+}]_i$ transient, and the tension-dependent binding of Ca^{2+} to TnC using a factorial analysis. Here we discuss the validation results, the implications of the factorial analysis, the sensitivity of the model to specific parameters, and the limitations of the model.

Validation

The model has been developed in components using specific experimental data, often recorded from experimental protocols specifically designed to isolate a particular mechanism or function. Model results have been successfully compared and validated against a combination of specific and physiological experimental results and normalized measures of tension kinetics.

Crossbridge kinetics were validated using rapid length-step experimental results from Kentish et al. (128) (see Fig. 9). The simulated results matched rapid length increases, but simulations for length-step decreases exhibited an unexpected rise in tension after the length step and no drop in steady-state tension after the length step was observed. The rise has been both present (132) and absent (130,136) in cardiac muscle experiments and has been observed in skeletal muscle (131). A potential explanation for the absence of the rise predicted by sinusoidal analysis (115) in quick release experiments is due to the buckling of the muscle during release (137). Buckling would not be observed in rapid stretch experiments and would be more likely to occur with larger length changes as Hancock et al. (130,136) used a 1% and 2% length change, compared to 0.05% used by Rossmanith and Tjokorda (131) and 0.5% used by de Beer et al. (132). Although no direct comparison can be made between model simulations and results by de Beer et al., who did not include the duration of the length step or provide a scale for tension. The rate constants used in the fading memory part of the HMT model are independent of $[Ca^{2+}]_i$ but the thin filament kinetics are not. So the effect of Ca^{2+} on the rate of tension redevelopment depends on $[Ca^{2+}]_i$, which

is not observed by Hancock et al. (130,136), but is seen by Backer et al. (138) and Wolff et al. (139). The second difference between simulations and experimental results was the absence of a decrease in steady-state tension after the length step. Significant decreases have been observed in ferret cardiac (130) and frog skeletal (140) muscle experimentally. In a critical review of this phenomenon, Rassier and Herzog (141) attributed the change in isometric tension to nonuniformity of *SL*s and stress-induced inhibition of crossbridge attachment after length steps. These observations are not accounted for by the model, due to the scarcity of specific data for cardiac tissue.

Ca^{2+} activation kinetics were defined using tension relaxation kinetics and F-pCa curves. Tension transients after the release of increasing concentrations of free Ca^{2+} were used to validate tropomyosin kinetics (see Fig. 8). The tension trace after the release of caged Ca^{2+} were closely followed by the simulated tension transients. The model was capable of representing a Ca^{2+}-dependent monoexponential rise in tension, while at the same time having a biphasic relaxation, as seen experimentally (61).

The complete model was compared with isometric twitch data from Janssen and de Tombe (133) with clamped and unclamped *SL* values (see Fig. 10). The model was able to replicate the tension traces, although the final phase of relaxation predicted by the model for both the clamped and unclamped twitch were slower than observed experimentally. In both cases, the use of experimental data recorded at 15°C to determine the tropomyosin relaxation parameters may have contributed to the delay in relaxation. In the unclamped case, the approximation of the force-velocity curve may also have caused reduced relaxation rates, as discussed below. The oscillations in the late phase of relaxation in the unclamped case is due to the imposed *SL*, which results in a forced *SL* velocity and the uncoupling of the feedback between velocity and tension. If the active contraction model was coupled to a passive mechanics model then the feedback between the passive and active mechanics would result in a smoother relaxation phase.

The model also quantitatively matches the increase in RT_{50} with increasing *SL* values, as seen experimentally by Janssen et al. (7) (see Fig. 11). An earlier study by Janssen and Hunter (4) using *SL* control to maintain the *SL* during contractions found lower RT_{50} values than both the model predictions and experimental results from Janssen et al. (7). However, only one data set is available from Janssen and Hunter (4) with $n = 1$, and no corresponding Ca^{2+} transient is provided. As such, a direct comparison is not possible. Janssen and Hunter (4) also reported that as *SL* decreased, the rate that tension fell from 25 to 10% of maximum tension increased. This phenomenon is not explicitly captured by the model, which predicts an increase in relaxation rate with *SL* within this range, although the model does predict an increase in relaxation rates for decreasing *SL* for larger *SL* values as tension drops from 35 to 25%.

The ability of the model to replicate specific tension twitches and RT_{50} trends supports the validity of the hypothesized model structure and parameter set.

Relaxation

The factorial analysis performed above highlighted the unbinding rate of Ca^{2+} from TnC and the $[Ca^{2+}]_i$ transient magnitude as the principle factors determining RT_{50}. The tension-dependent binding of Ca^{2+} to TnC and the length-dependent Ca^{2+} sensitivity played a secondary role and maximum tension and two-factor interactions did not significantly affect RT_{50} values in the examined parameter space.

The effect of an increase in the unbinding rate of Ca^{2+} from TnC on the relaxation has been studied experimentally by phosphorylating troponin I using protein kinase A, causing $\approx$30% increase in the unbinding rate of Ca^{2+} from TnC (6,92). The increase in unbinding rate has been shown to cause a decrease in RT_{50} in intact preparations (142) and both an increase (6,61) and no effect (64) in the rate of relaxation in skinned preparations, using light-activated Ca^{2+} chelators. The factorial analysis identified the unbinding of Ca^{2+} from TnC as a significant determinant of relaxation.

The effect of *SL* on RT_{50} was separated into the length dependence of tension and calcium sensitivity. The *SL* tension dependence had a minimal affect on RT_{50}, whereas the length-dependent calcium sensitivity had a significant affect on RT_{50}. Experimental results from Janssen and Hunter (3) found tension and not *SL* correlated with relaxation times, suggesting that either the tension dependence of Ca^{2+} binding to TnC or that bound crossbridges inhibit tropomyosin returning to the off-state, are responsible for the increase in relaxation time with *SL*. Kentish and Wrzosek (143) and Janssen et al. (7) also recorded a decrease in RT_{50} at shorter *SL*s, but the effect of *SL* would also be confounded by changes in the tension transient, which potentially causes changes in the binding of Ca^{2+} to TnC and thus has an effect on the relaxation time. The Ca^{2+} sensitivity affects both maximum tension and RT_{50}, coinciding with the observations of Janssen and Hunter (4). However, since no definitive mechanism currently exists to explain the length-dependent Ca^{2+} sensitivity as discussed above, the dependence of RT_{50} on Ca^{2+} sensitivity cannot be determined.

Model simulations show that RT_{50} increases with the $[Ca^{2+}]_i$ transient magnitude, when the $[Ca^{2+}]_i$ transient and the unbinding rate of Ca^{2+} from TnC are close to their reference values. Increasing the extracellular Ca^{2+} concentration, which increases the $[Ca^{2+}]_i$ transient magnitude, has been observed to cause an increase (3,4), a decrease (3), and no change (144) in relaxation rates. Fig. 12 *B* shows the combined effects of the unbinding rate and the $[Ca^{2+}]_i$ transient magnitude on RT_{50}. The $[Ca^{2+}]_i$ transient causes both a decrease and an increase in RT_{50}, as seen by Gao et al. (3), depending on the $[Ca^{2+}]_i$ transient magnitude and the unbinding rate of Ca^{2+} from TnC.

The unbinding of Ca^{2+} from TnC and the $[Ca^{2+}]_i$ transient are the most significant factors in determining RT_{50}. The coupled effects of TnC and the $[Ca^{2+}]_i$ transient on RT_{50} were determined using a broader range of parameter values (see Fig. 12 *B*) and showed that the minimum RT_{50} was a function of both the $[Ca^{2+}]_i$ transient and the unbinding rate of Ca^{2+} from TnC, such that the effect of the $[Ca^{2+}]_i$ transient and the unbinding rate of Ca^{2+} from TnC could both either increase or decrease RT_{50} depending on the reference value of each parameter. For example, for the base $[Ca^{2+}]_i$ transient, increasing the unbinding rate of Ca^{2+} from TnC increase or decreases RT_{50} when the unbinding rate is more or less than 130%, respectively.

Sarcomere velocity and crossbridges inhibiting the movement of tropomyosin to the off-state were not included in this study. To attain realistic tension twitches, where the muscle contracts, requires the use of physiological force boundary conditions. To account for the affect of *SL* velocity under this protocol requires the definition of a passive stiffness model, which is beyond the scope of this article. Crossbridge inhibition is not accounted for explicitly, and could potentially affect a number of tropomyosin kinetics parameters (α_{r2}, n_r, K_z). Crossbridge inhibition may, in part, account for the significant effect of the $[Ca^{2+}]_i$ transient on RT_{50}, and may need to be considered at a later date.

Sensitivity

The model described above contains numerous parameters defined using a range of experimental data. To fully assess the validity of the model, the sensitivity of model results to individual parameters needed to be determined. The relevance and quality of data used to determine sensitive parameters was then assessed to attain a sense of the accuracy and degree of confidence in the model.

The sensitivity of the model to specific parameters was determined by calculating the Jacobean of the root-mean-square change in tension (for the unclamped sarcomere tension trace), with respect to the parameter set. The tension transient was most sensitive to $Ca_{Trpn50ref}$ and K_z, and insensitive to changes in either the crossbridge kinetics or Ca^{2+} binding to TnC.

$Ca_{Trpn50ref}$ was determined using the Ca^{2+} bound to TnC model and free Ca^{2+} (Eq. 12) at half-activation values from skinned and intact preparations. The $Ca_{Trpn50ref}$ value for skinned preparations was calculated from 17 experiments at different *SL* values. However, adjusting $Ca_{Trpn50ref}$ to account for the affects of skinning used only three measures at one *SL* and the effect of skinning on the length dependence of half-activation was assumed to be negligible. To confirm the validity of the value and length dependence of $Ca_{Trpn50ref}$, further experiments on intact preparations are required as, although many factors have been qualitatively implicated in determining the effects of skinning on the half-activation, there is currently no established relationship between skinned and intact half-activation values.

The value K_z was defined by fitting Eq. 14 to tension transients after step changes in Ca^{2+}. The value K_z was determined by fitting a nonlinear equation to characteristic tension traces and our confidence in its value is therefore less than parameters directly reported in the literature, which are taken from numerous samples. The experiments used to determine K_z were also performed at 12–15°C in air and the tension reached during the experiment was commonly 50% of the maximum tension. Further experiments at more physiological temperatures over a broader range of tensions would assist in better defining K_z to increase the validity of the model and conclusions drawn from it.

Limitations

This model aims to account for a wide range of experimental results and mechanisms. Although the model is capable of representing a large proportion of available experimental data, it is an approximation, and as such, has limitations, which must be taken into consideration when considering results. In the model, certain components have a limited representation of experimental results and some potential mechanisms were not included. These include: the length- and tension-dependence of Ca^{2+} binding to TnC, the changes in half-activation due to skinning, relying on the approximation of the Hill equation, the models' approximation of the F-pCa curve, and inhomogeneous sarcomere shortening in relaxation, which are discussed below.

The tension-dependent binding of Ca^{2+} to TnC is only valid for the physiological range of *SL* values and fails to predict the concentration of bound Ca^{2+} during contraction at low free Ca^{2+} concentrations. The model is designed to operate within the physiological range of *SL* values for intact preparations between $1.8 < SL < 2.3\ \mu$m. Extensions beyond 2.3 μm do not occur under physiological conditions in vivo. Simulating isolated experimental protocols where $SL > 2.3\mu$m, the model will predict that more than one Ca^{2+} ion binding to each available site II in TnC as k_{off} becomes less than zero, which is not reported. For simulations where $SL < 2.3\ \mu$m, $k_{off} > 0$ if $T < \gamma T_{ref}$ for all tension values, resulting in the condition that $\gamma > 1 + \beta_0(\lambda - 1)$, which is true for the proposed parameter set. Combining the active tension model described here with a model for passive tension (11) would constrain *SL*s to be below 2.3 μm and so avoid this problem. The fraction of Ca^{2+} bound to TnC at lower *SL* values reported by Fuchs et al. (44) is not accurately represented by the model. However, there is an amplification of experimental noise inherent in the method used here to extrapolate the fraction of Ca^{2+} bound to site II from the experimental results (discussed in the Tension-Dependent Ca^{2+} unbinding rate from Troponin C) which increases as bound Ca^{2+} decreases. This impedes the accurate measurement Ca^{2+} bound to site II

using the total quantity of Ca^{2+} bound to all TnC sites as the sole source of experimental data.

The half-activation of cardiac muscle is often reduced after skinning. Here the half-activation is scaled to match intact preparation data, but the half-activation length dependence (β_0) is not defined for intact preparations and as such it is assumed to be independent of skinning. Further experiments on the length dependence of Ca^{2+} activation would help to elucidate which parts of the contractile machinery are affected by the skinning process.

Crossbridge kinetics after a length perturbation was described by the fading memory model. The static nonlinear component of the fading memory model is described by the Hill equation. The Hill equation exhibits two problems. Firstly, the Hill curve has been shown to be insufficient to represent experimental force-velocity results for small velocities (111). Secondly, the force-velocity relationship for negative velocities is not described by the Hill curve, which is therefore extended here to cover both positive and negative velocities. Further experimental evidence is required to appropriately characterize the force velocity curve for negative velocities.

The steady-state F-pCa curve (see Fig. 5) is steeper for midlevel [Ca^{2+}] than low and high [Ca^{2+}], which is a problem endemic in mean-field-averaged models as noted by Rice and de Tombe (76). A potential solution to this problem is the explicit representation of the regulatory proteins as proposed by Rice and de Tombe, but this method is not currently computationally feasible for the simulations performed here.

Recent tension transients after a rapid drop in local Ca^{2+} recorded by Stehele et al. (5,145) and Belus et al. (146) did not contain the fast and slow processes seen in light-activated Ca^{2+} chelator experiments. Stehele et al. and Belus et al. found an initial linear relaxation phase followed by exponential relaxation similar to that seen in skeletal muscle (100). The initial linear phase is most pronounced in the absence of P_i. However, the linear phase is muted when P_i is at physiological concentrations of 2 mM (146), and therefore is not considered in this model.

Our results reveal the importance of the $[Ca^{2+}]_i$ transient and unbinding of Ca^{2+} from TnC as the significant factors affecting RT_{50}. The tension dependence of Ca^{2+} binding to TnC and length-dependent Ca^{2+} have a lesser affect and length-dependent maximum tension appears to have a minimal influence on RT_{50}. A sensitivity analysis of the tension transient found simulation results to be most sensitive to tropomyosin kinetics, but this does not detract from the principal finding that the $[Ca^{2+}]_i$ transient and the unbinding of Ca^{2+} from TnC are the significant factors in determining the relaxation of cardiac muscle, based on the current understanding of cardiac contraction.

Applications

In this study, a model was developed to rationalize a wide range of experimental data and to rationalize the mechanisms that control relaxation. The efficient computational form of the model allows it to be applied to both single and multicellular simulations. For example, the active mechanics model described here has been incorporated into continuum models of tissue to determine large deformation mechanics solutions and, ultimately, coupled electromechanics interactions within the heart. This will ultimately provide the ability to link cellular mechanisms in health and pathological states to whole organ function and, in doing so, further the goals of integrative physiology efforts such as the IUPS physiome project (147).

SUMMARY

A wide range of experimental results has been surveyed to provide a parameter set for the HMT model, which coincides with the majority of reported experimental results. The model illustrates the importance of the coupled effects of the Ca^{2+} transient and the unbinding rate of Ca^{2+} from TnC on the rate of relaxation and the limited effects of SL on RT_{50}. The model tension traces are most sensitive to the bound Ca^{2+} at half-activation in intact preparations and K_z. Further experiments characterizing the length dependence of half-activation in intact preparations and relaxation kinetics performed under more physiological conditions over a wider range of tensions would assist in improving the confidence in model results. The model is designed to be applied in multiscale tissue and organ simulations, which is necessary to gain further understanding of the effects of tissue and passive mechanics on relaxation.

Data from experimental studies used to validate the model are listed. A full description of the model is available using the CellML ontology at www.cellml.org/examples/maths_pdf/NHS_maths.pdf (148).

Richard Faville and Dr. Rob Kirton provided assistance with digitizing and muscle physiology, respectively.

S.N. thanks the New Zealand Institute of Mathematics and its Applications, the William Georgetti Trust, the Tertiary Education Commission, and the New Zealand Heart Foundation. N.S. thanks the Royal Society of New Zealand and the Marsden Fund for providing funding for this research. P.H. is grateful to the Wellcome Trust.

REFERENCES

1. McIvor, M., C. Orchard, and E. Lakatta. 1988. Dissociation of changes in apparent myofibrillar Ca^{2+} sensitivity and twitch relaxation induced by adrenergic and cholinergic stimulation in isolated ferret cardiac muscle. *J. Gen. Physiol.* 92:509–529.
2. Backx, P. H., W. D. Gao, M. D. Azanbackx, and E. Marban. 1995. The relationship between contractile-force and intracellular Ca^{2+} in intact rat cardiac trabeculae. *J. Gen. Physiol.* 105:1–19.
3. Gao, W. D., N. G. Perez, and E. Marban. 1998. Calcium cycling and contractile activation in intact mouse cardiac muscle. *J. Physiol. (Lond.).* 507:175–184.
4. Janssen, P. M., and W. C. Hunter. 1995. Force, not sarcomere length, correlates with prolongation of isosarcometric contraction. *Am. J. Physiol.* 269:H676–H685.
5. Stehle, R., M. Kruger, and G. Pfitzer. 2002. Force kinetics and individual sarcomere dynamics in cardiac myofibrils after rapid Ca^{2+} changes. *Biophys. J.* 83:2152–2161.

6. Zhang, R., J. Zhao, A. Mandveno, and J. D. Potter. 1995. Cardiac Troponin I phosphorylation increases the rate of cardiac muscle relaxation. *Circ. Res.* 76:1028–1035.
7. Janssen, P. M. L., L. B. Stull, and E. Marban. 2002. Myofilament properties comprise the rate-limiting step for cardiac relaxation at body temperature in the rat. *Am. J. Physiol.* 282:H499–H507.
8. Rice, J. J., M. S. Jafri, and R. L. Winslow. 2000. Modeling short-term interval-force relations in cardiac muscle. *Am. J. Physiol.* 278:H913–H931.
9. Smith, N. P., M. L. Buist, and A. J. Pullan. 2003. Altered T-wave dynamics in a contracting cardiac model. *J. Cardiovasc. Electrophysiol.* 14:S203–S209.
10. Kerckhoffs, R.C.P., O.P. Faris, P.H.M. Bovendeerd, F.W. Prinzen, K. Smits, E.R. McVeigh, and T. Arts. 2003. Timing of depolarization and contraction in the paced canine left ventricle: model and experiment. *J. Cardiovasc. Electrophysiol.* 14:S188–S195.
11. Hunter, P. J., A. D. McCulloch, and H. ter Keurs. 1998. Modelling the mechanical properties of cardiac muscle. *Prog. Biophys. Mol. Biol.* 69:289–331.
12. Solaro, R.J., and H.M. Rarick. 1998. Troponin and tropomyosin: proteins that switch on and tune in the activity of cardiac myofilaments. *Circ. Res.* 83:471–480.
13. Holroyde, M. J., S. P. Robertson, J. D. Johnson, R. J. Solaro, and J. D. Potter. 1980. The calcium and magnesium binding-sites on cardiac troponin and their role in the regulation of myofibrillar adenosine-triphosphatase. *J. Biol. Chem.* 255:1688–1693.
14. Robertson, S. P., J. D. Johnson, and J. D. Potter. 1981. The timecourse of Ca^{2+} exchange with calmodulin, troponin, parvalbumin, and myosin in response to transient increases in Ca^{2+}. *Biophys. J.* 34:559–569.
15. Fabiato, A. 1983. Calcium-induced release of calcium from the cardiac sarcoplasmic reticulum. *Am. J. Physiol.* 245:C1–C14.
16. Solaro, R. J., R. M. Wise, J. S. Shiner, and F. N. Briggs. 1974. Calcium requirements for cardiac myofibrillar activation. *Circ. Res.* 34:525–530.
17. Gillis, T. E., C. R. Marshall, X. H. Xue, T. J. Borgford, and G. F. Tibbits. 2000. Ca^{2+} binding to cardiac troponin C: effects of temperature and pH on mammalian and salmonid isoforms. *Am. J. Physiol.* 279:R1707–R1715.
18. Li, M. X., S. M. Gagne, L. Spyracopoulos, C. Kloks, G. Audette, M. Chandra, R. J. Solaro, L. B. Smillie, and B. D. Sykes. 1997. NMR studies of Ca^{2+} binding to the regulatory domains of cardiac and E41A skeletal muscle troponin C reveal the importance of site I to energetics of the induced structural changes. *Biochemistry.* 36:12519–12525.
19. Gillis, T. E., C. D. Moyes, and G. F. Tibbits. 2003. Sequence mutations in teleost cardiac troponin C that are permissive of high Ca^{2+} affinity of site II. *Am. J. Physiol.* 284:C1176–C1184.
20. Dong, W. J., S. S. Rosenfeld, C. K. Wang, A. M. Gordon, and H. C. Cheung. 1996. Kinetic studies of calcium binding to the regulatory site of troponin C from cardiac muscle. *J. Biol. Chem.* 271:688–694.
21. Wattanapermpool, J., P .J. Reiser, and R. J. Solaro. 1995. Troponin-I isoforms and differential effects of acidic pH on soleus and cardiac myofilaments. *Am. J. Physiol.* 37:C323–C330.
22. Putkey, J. A., W. Liu, X. Lin, S. Ahmed, M. Zhang, J. D. Potter, and W. G. L. Kerrick. 1997. Fluorescent probes attached to Cys-35 or Cys-84 in cardiac troponin C are differentially sensitive to Ca^{2+}-dependent events in vitro and in situ. *Biochemistry.* 36:970–978.
23. Johnson, J. D., J. H. Collins, S. P. Robertson, and J. D. Potter. 1980. A fluorescent-probe study of Ca^{2+} binding to the Ca^{2+}-specific sites of cardiac troponin and troponin-C. *J. Biol. Chem.* 255:9635–9640.
24. Li, M. X., E. J. Saude, X. Wang, J. R. Pearlstone, L. B. Smillie, and B. D. Sykes. 2002. Kinetic studies of calcium and cardiac troponin I peptide binding to human cardiac troponin C using NMR spectroscopy. *Eur. Biophys. J.* 31:245–256.
25. Tikunova, S. B., and J. P. Davis. 2004. Designing calcium-sensitizing mutations in the regulatory domain of cardiac troponin C. *J. Biol. Chem.* 279:35341–35352.
26. Li, G., A. F. Martin, and R. J. Solaro. 2001. Localization of regions of troponin I important in deactivation of cardiac myofilaments by acidic pH. *J. Mol. Cell. Cardiol.* 33:1309–1320.
27. Tobacman, L. S., and D. Sawyer. 1990. Calcium binds cooperatively to the regulatory sites of the cardiac thin filament. *J. Biol. Chem.* 265: 931–939.
28. Pan, B. S., and R. J. Solaro. 1987. Calcium-binding properties of troponin-C in detergent-skinned heart muscle fibers. *J. Biol. Chem.* 262:7839–7849.
29. Parsons, B., D. Szczesna, J. J. Zhao, G. VanSlooten, W. G. L. Kerrick, J. A. Putkey, and J. D. Potter. 1997. The effect of pH on the Ca^{2+} affinity of the Ca^{2+} regulatory sites of skeletal and cardiac troponin-C in skinned muscle fibres. *J. Muscle Res. Cell Motil.* 18: 599–609.
30. Wnuk, W., M. Schoechlin, and E. Stein. 1984. Regulation of actomyosin ATPase by a single calcium-binding site on troponin C from crayfish. *J. Biol. Chem.* 259:9017–9023.
31. Fujino, K., N. Sperelakis, and R. J. Solaro. 1988. Sensitization of dog and guinea-pig heart myofilaments to Ca^{2+} activation and the inotropic effect of pimobendan—comparison with milrinone. *Circ. Res.* 63:911–922.
32. Hofmann, P. A., and F. Fuchs. 1988. Bound calcium and force development in skinned cardiac muscle bundles—effect of sarcomere-length. *J. Mol. Cell. Cardiol.* 20:667–677.
33. Hofmann, P. A., and F. Fuchs. 1987. Evidence for a force-dependent component of calcium-binding to cardiac troponin-C. *Am. J. Physiol.* 253:C541–C546.
34. Hofmann, P. A., and F. Fuchs. 1987. Bound Ca^{2+} and force development in detergent-extracted cardiac muscle bundles—effect of sarcomere length. *Biophys. J.* 51:A463.
35. Ball, K. L., M. D. Johnson, and R. J. Solaro. 1994. Isoform-specific interactions of Troponin-I and Troponin-C determine pH sensitivity of myofibrillar Ca^{2+} activation. *Biochemistry.* 33:8464–8471.
36. Potter, J. D., J. C. Seidel, P. Leavis, S. S. Lehrer, and J. Gergely. 1976. Effect of Ca^{2+} binding on troponin C. Changes in spin label mobility, extrinsic fluorescence, and sulfhydryl reactivity. *J. Biol. Chem.* 251:7551–7556.
37. Potter, J. D., and J. Gergely. 1975. The calcium and magnesium binding sites on troponin and their role in the regulation of myofibrillar adenosine triphosphatase. *J. Biol. Chem.* 250:4628–4633.
38. Fuchs, F., and Y. P. Wang. 1996. Sarcomere length versus interfilament spacing as determinants of cardiac myofilament Ca^{2+} sensitivity and Ca^{2+} binding. *J. Mol. Cell. Cardiol.* 28:1375–1383.
39. Fuchs, F., M. E. Whaley, and P. A. Hofmann. 1988. Binding of Ca^{2+} to skinned muscle fibers at short sarcomere length—comparison of skeletal and cardiac muscle. *Biophys. J.* 53:A566–A566.
40. Hofmann, P. A., and F. Fuchs. 1985. The effect of sarcomere length on Ca^{2+} sensitivity and Ca^{2+}-binding in detergent-extracted cardiac muscle bundles. *Biophys. J.* 47:A290.
41. Hofmann, P. A., and F. Fuchs. 1987. Effect of length and cross-bridge attachment on Ca^{2+} binding to cardiac troponin-C. *Am. J. Physiol.* 253:C90–C96.
42. Wang, Y. P., and F. Fuchs. 1995. Osmotic compression of skinned cardiac and skeletal muscle bundles—effects on force generation, Ca^{2+} sensitivity and Ca^{2+} binding. *J. Mol. Cell. Cardiol.* 27: 1235–1244.
43. Wang, Y. P., and F. Fuchs. 2001. Interfilament spacing, Ca^{2+} sensitivity, and Ca^{2+} binding in skinned bovine cardiac muscle. *J. Muscle Res. Cell Motil.* 22:251–257.
44. Wang, Y. P., and F. Fuchs. 1994. Length, force, and Ca^{2+}-troponin-C affinity in cardiac and slow skeletal muscle. *Am. J. Physiol.* 266: C1077–C1082.
45. Kentish, J. C., H. Terkeurs, L. Ricciardi, J. J. J. Bucx, and M. I. M. Noble. 1986. Comparison between the sarcomere length-force relations of intact and skinned trabeculae from rat right ventricle—influence of calcium concentrations on these relations. *Circ. Res.* 58:755–768.

46. Dobesh, D. P., J. P. Konhilas, and P. P. de Tombe. 2002. Cooperative activation in cardiac muscle: impact of sarcomere length. *Am. J. Physiol.* 282:H1055–H1062.

47. Rosenfeld, S. S., and E. W. Taylor. 1985. Kinetic studies of calcium-binding to regulatory complexes from skeletal muscle. *J. Biol. Chem.* 260:252–261.

48. Dong, W. J., C. K. Wang, A. M. Gordon, S. S. Rosenfeld, and H. C. Cheung. 1997. A kinetic model for the binding of Ca^{2+} to the regulatory site of troponin from cardiac muscle. *J. Biol. Chem.* 272: 19229–19235.

49. Smith, S. J., and P. J. England. 1990. The effects of reported Ca^{2+} sensitizers on the rates of Ca^{2+} release from cardiac troponin-C and the troponin-tropomyosin complex. *Br. J. Pharmacol.* 100:779–785.

50. Johnson, J. D., R. J. Nakkula, C. Vasulka, and L. B. Smillie. 1994. Modulation of Ca^{2+} exchange with the Ca^{2+}-specific regulatory sites of troponin-C. *J. Biol. Chem.* 269:8919–8923.

51. Luo, Y., J. P. Davis, L. B. Smillie, and J. A. Rall. 2002. Determinants of relaxation rate in rabbit skinned skeletal muscle fibres. *J. Physiol.* (*Lond.*). 545:887–901.

52. Brenkelmann, D., J. D. Potter, and P. R. Housmans. 2002. Effects of volatile anesthetics on kinetics of conformational changes after Ca^{2+} dissociation from human recombinant cardiac troponin C. *Biophys. J.* 82:387A.

53. Hazard, A. L., S. C. Kohout, N. L. Stricker, J. A. Putkey, and J. J. Falke. 1998. The kinetic cycle of cardiac troponin C: calcium binding and dissociation at site II trigger slow conformational rearrangements. *Protein Sci.* 7:2451–2459.

54. Johnson, J. D., J. H. Collins, and J. D. Potter. 1978. Dansylaziridine-labeled troponin C. A fluorescent probe of Ca^{2+} binding to the Ca^{2+}-specific regulatory sites. *J. Biol. Chem.* 253:6451–6458.

55. Allen, D. G., and S. Kurihara. 1982. The effects of muscle length on intracellular calcium transients in mammalian cardiac-muscle. *J. Physiol.* (*Lond.*). 327:79–94.

56. Allen, D. G., and J. C. Kentish. 1988. Calcium-concentration in the myoplasm of skinned ferret ventricular muscle following changes in muscle length. *J. Physiol.* (*Lond.*). 407:489–503.

57. Komukai, K., T. Ishikawa, and S. Kurihara. 1998. Effects of acidosis on Ca^{2+} sensitivity of contractile elements in intact ferret myocardium. *Am. J. Physiol.* 274:H147–H154.

58. Lee, J. A., and D. G. Allen. 1991. EMD-53998 sensitizes the contractile proteins to calcium in intact ferret ventricular muscle. *Circ. Res.* 69:927–936.

59. Yagi, N., H. Okuyama, H. Toyota, J. Araki, J. Shimizu, G. Iribe, K. Nakamura, S. Mohri, K. Tsujioka, H. Suga, and F. Kajiya. 2004. Sarcomere-length dependence of lattice volume and radial mass transfer of myosin cross-bridges in rat papillary muscle. *Pflueg. Arch. Eur. J. Physiol.* 448:153–160.

60. Saeki, Y., T. Kobayashi, S.-I. Yasuda, S. Nishimura, S. Sugiura, H. Yamashita, and H. Sugi. 2004. Role of Ca^{2+} in determining the rate of tension development and relaxation in rat skinned myocardium. *J. Mol. Cell. Cardiol.* 36:371–380.

61. Saeki, Y., K. Takigiku, H. Iwamoto, S. Yasuda, H. Yamashita, S. Sugiura, and H. Sugi. 2001. Protein kinase A increases the rate of relaxation but not the rate of tension development in skinned rat cardiac muscle. *Jpn. J. Physiol.* 51:427–433.

62. Fitzsimons, D. P., J. R. Patel, and R. L. Moss. 1998. Role of myosin heavy chain composition in kinetics of force development and relaxation in rat myocardium. *J. Physiol.* (*Lond.*). 513:171–183.

63. Palmer, S., and J. C. Kentish. 1997. Differential effects of the Ca^{2+} sensitizers caffeine and CGP 48506 on the relaxation rate of rat skinned cardiac trabeculae. *Circ. Res.* 80:682–687.

64. Johns, E. C., S. J. Simnett, I. P. Mulligan, and C. C. Ashley. 1997. Troponin I phosphorylation does not increase the rate of relaxation following laser flash photolysis of diazo-2 in guinea-pig skinned trabeculae. *Pflueg. Arch. Eur. J. Physiol.* 433:842–844.

65. Simnett, S. J., E. C. Johns, S. Lipscomb, I. P. Mulligan, and C. C. Ashley. 1998. Effect of pH, phosphate, and ADP on relaxation of myocardium after photolysis of diazo-2. *Am. J. Physiol.* 275:H951–H960.

66. Palmer, S., and J. C. Kentish. 1998. Roles of Ca^{2+} and crossbridge kinetics in determining the maximum rates of Ca^{2+} activation and relaxation in rat and guinea pig skinned trabeculae. *Circ. Res.* 83: 179–186.

67. Akella, A. B., H. Su, E. H. Sonnenblick, V. G. Rao, and J. Gulati. 1997. The cardiac troponin-C isoform and the length dependence of Ca^{2+} sensitivity of tension in myocardium. *J. Mol. Cell. Cardiol.* 29: 381–389.

68. Babu, A., E. H. Sonnenblick, and J. Gulati. 1996. Altered interactions among thin filament proteins modulate cardiac function: a clarification. *J. Mol. Cell. Cardiol.* 28:1829–1830.

69. Gulati, J., E. Sonnenblick, and A. Babu. 1991. The role of troponin-C in the length dependence of Ca^{2+}-sensitive force of mammalian skeletal and cardiac muscles. *J. Physiol.* (*Lond.*). 441:305–324.

70. Babu, A., E. Sonnenblick, and J. Gulati. 1988. Molecular basis for the influence of muscle length on myocardial performance. *Science.* 240:74–76.

71. Fitzsimons, D. P., and R. L. Moss. 1998. Strong binding of myosin modulates length-dependent Ca^{2+} activation of rat ventricular myocytes. *Circ. Res.* 83:602–607.

72. Fukuda, N., D. Sasaki, S. Ishiwata, and S. Kurihara. 2001. Length dependence of tension generation in rat skinned cardiac muscle: role of titin in the Frank-Starling mechanism of the heart. *Circulation.* 104:1639–1645.

73. McDonald, K. S., and R. L. Moss. 1995. Osmotic compression of single cardiac myocytes eliminates the reduction in Ca^{2+} sensitivity of tension at short sarcomere-length. *Circ. Res.* 77: 199–205.

74. Konhilas, J., T. Irving, and P. P. de Tombe. 2002. Myofilament calcium sensitivity in skinned rat cardiac trabeculae: role of interfilament spacing. *Circ. Res.* 90:59–65.

75. Moss, R. L., and D. P. Fitzsimons. 2002. Frank-Starling relationship: long on importance, short on mechanism. *Circ. Res.* 90:11–13.

76. Rice, J. J., and P. P. de Tombe. 2004. Approaches to modeling crossbridges and calcium-dependent activation in cardiac muscle. *Prog. Biophys. Mol. Biol.* 85:179–195.

77. Hibberd, M. G., and B. R. Jewell. 1982. Calcium-dependent and length-dependent force production in rat ventricular muscle. *J. Physiol.* (*Lond.*). 329:527–540.

78. Wannenburg, T., P. M. L. Janssen, D. Fan, and P. P. De Tombe. 1997. The Frank-Starling mechanism is not mediated by changes in rate of cross-bridge detachment. *Am. J. Physiol.* 273:H2428–H2435.

79. Sweitzer, N., and R. Moss. 1990. The effect of altered temperature on Ca^{2+}-sensitive force in permeabilized myocardium and skeletal muscle. Evidence for force dependence of thin filament activation. *J. Gen. Physiol.* 96:1221–1245.

80. Ebus, J. P., Z. Papp, R. Zaremba, and G. J. M. Stienen. 2001. Effects of MgATP on ATP utilization and force under normal and simulated ischaemic conditions in rat cardiac trabeculae. *Pflueg. Arch. Eur. J. Physiol.* 443:102–111.

81. Martin, H., M. G. Bell, G. C. R. Ellis-Davies, and R. J. Barsotti. 2004. Activation kinetics of skinned cardiac muscle by laser photolysis of nitrophenyl-EGTA. *Biophys. J.* 86:978–990.

82. Wannenburg, T., G. H. Heijne, J. H. Geerdink, H. W. Van den Dool, P. M. L. Janssen, and P. P. De Tombe. 2000. Cross-bridge kinetics in rat myocardium: effect of sarcomere length and calcium activation. *Am. J. Physiol.* 279:H779–H790.

83. Konhilas, J. P., T. C. Irving, and P. P. de Tombe. 2002. Length-dependent activation in three striated muscle types of the rat. *J. Physiol.* (*Lond.*). 544:225–236.

84. Hofmann, P. A., and R. L. Moss. 1992. Effects of calcium on shortening velocity in frog chemically skinned atrial myocytes and in

mechanically disrupted ventricular myocardium from rat. *Circ. Res.* 70:885–892.

85. Fujita, H., and S. Ishiwata. 1999. Tropomyosin modulates pH dependence of isometric tension. *Biophys. J.* 77:1540–1546.
86. Cazorla, O., G. Vassort, D. Garnier, and J.-Y. Le Guennec. 1999. Length modulation of active force in rat cardiac myocytes: is titin the sensor? *J. Mol. Cell. Cardiol.* 31:1215–1227.
87. Ventura-Clapier, R., H. Mekhfi, and G. Vassort. 1987. Role of creatine kinase in force development in chemically skinned rat cardiac muscle. *J. Gen. Physiol.* 89:815–837.
88. Papp, Z., A. Szabo, J. P. Barends, and G. J. M. Stienen. 2002. The mechanism of the force enhancement by MgADP under simulated ischaemic conditions in rat cardiac myocytes. *J. Physiol.* (*Lond.*). 543:177–189.
89. Gao, W. D., P. H. Backx, M. Azanbackx, and E. Marban. 1994. Myofilament Ca^{2+} sensitivity in intact versus skinned rat ventricular muscle. *Circ. Res.* 74:408–415.
90. Harris, S. P., J. R. Patel, L J. Marton, and R. L. Moss. 2000. Polyamines decrease Ca^{2+} sensitivity of tension and increase rates of activation in skinned cardiac myocytes. *Am. J. Physiol.* 279:H1383–H1391.
91. Zot, H., K. Guth, and J. Potter. 1986. Fast skeletal muscle skinned fibers and myofibrils reconstituted with N- terminal fluorescent analogues of troponin C. *J. Biol. Chem.* 261:15883–15890.
92. Robertson, S. P., J. D. Johnson, M. J. Holroyde, E. G. Kranias, J. D. Potter, and R. J. Solaro. 1982. The effect of Troponin-I phosphorylation on the Ca^{2+}-binding properties of the Ca^{2+}-regulatory site of bovine cardiac troponin. *J. Biol. Chem.* 257:260–263.
93. Andrews, M., D. Maughan, T. Nosek, and R. Godt. 1991. Ion-specific and general ionic effects on contraction of skinned fast-twitch skeletal muscle from the rabbit. *J. Gen. Physiol.* 98:1105–1125.
94. Coomber, S. J., E. Tarasewicz, and G. F. Elliott. 1999. Calcium dependence of Donnan potentials in rigor: the effects of Mg^{2+} and anions in isolated rabbit psoas muscle fibres. *Cell Calcium.* 25:43–57.
95. Gao, W. D., D. Atar, P. H. Backx, and E. Marban. 1995. Relationship between intracellular calcium and contractile force in stunned myocardium—direct evidence for decreased myofilament Ca^{2+} responsiveness and altered diastolic function in intact ventricular muscle. *Circ. Res.* 76:1036–1048.
96. Yue, D., E. Marban, and W. Wier. 1986. Relationship between force and intracellular [Ca^{2+}] in tetanized mammalian heart muscle. *J. Gen. Physiol.* 87:223–242.
97. Irving, T. C., J. Konhilas, D. Perry, R. Fischetti, and P. P. de Tombe. 2000. Myofilament lattice spacing as a function of sarcomere length in isolated rat myocardium. *Am. J. Physiol.* 279:H2568–2573.
98. Stephenson, D. G. 2003. Relationship between isometric force and myofibrillar MgATPase at short sarcomere length in skeletal and cardiac muscle and its relevance to the concept of activation heat. *Clin. Exp. Pharmacol. Physiol.* 30:570–575.
99. Konhilas, J., T. Irving, and P. de Tombe. 2002. Frank-Starling law of the heart and the cellular mechanisms of length-dependent activation. *Pflueg. Arch. Eur. J. Physiol.* 445:305–310.
100. Woledge, R. C., N. A. Curtin, and E. Homsher. 1985. Energetic Aspects of Muscle Contraction. Academic Press, London.
101. Lim, C. C., M. H. B. Helmes, D. B. Sawyer, M. Jain, and R. Liao. 2001. High-throughput assessment of calcium sensitivity in skinned cardiac myocytes. *Am. J. Physiol.* 281:H969–H974.
102. Kirton, R. S., A. J. Taberner, P. M. F. Nielsen, A. A. Young, and D. S. Loiselle. 2004. Strain softening behaviour in nonviable rat right-ventricular trabeculae, in the presence and the absence of butanedione monoxime. *Exp. Physiol.* 89:593–604.
103. Vahl, C.F., T. Timek, A. Bonz, H. Fuchs, R. Dillman, and S. Hagl. 1998. Length dependence of calcium- and force-transients in normal and failing human myocardium. *J. Mol. Cell. Cardiol.* 30:957–966.
104. Wolska, B. M., K. Vijayan, G. M. Arteaga, J. P. Konhilas, R. M. Phillips, R. Kim, T. Naya, J. M. Leiden, A. F. Martin, P. P. de Tombe, and R. J. Solaro. 2001. Expression of slow skeletal troponin I in adult transgenic mouse heart muscle reduces the force decline observed during acidic conditions. *J. Physiol.* (*Lond.*). 536:863–870.
105. de Tombe, P. P., and H. ter Keurs. 1991. Sarcomere dynamics in cat cardiac trabeculae. *Circ. Res.* 68:588–596.
106. Ricciardi, L., R. Bottinelli, M. Canepari, and C. Reggiani. 1994. Effects of acidosis on maximum shortening velocity and force-velocity relation of skinned rat cardiac muscle. *J. Mol. Cell. Cardiol.* 26:601–607.
107. de Tombe, P. P., and H. ter Keurs. 1992. An internal viscous element limits unloaded velocity of sarcomere shortening in rat myocardium. *J. Physiol.* (*Lond.*). 454:619–642.
108. Herron, T. J., F. S. Korte, and K. S. McDonald. 2001. Loaded shortening and power output in cardiac myocytes are dependent on myosin heavy chain isoform expression. *Am. J. Physiol.* 281:H1217–H1222.
109. Diffee, G. M., and E. Chung. 2003. Altered single cell force-velocity and power properties in exercise-trained rat myocardium. *J. Appl. Physiol.* 94:1941–1948.
110. Hinken, A. C., and K. S. McDonald. 2004. Inorganic phosphate speeds loaded shortening in rat skinned cardiac myocytes. *Am. J. Physiol.* 287:C500–C507.
111. de Tombe, P. P., and H. ter Keurs. 1990. Force and velocity of sarcomere shortening in trabeculae from rat heart—effects of temperature. *Circ. Res.* 66:1239–1254.
112. Oiwa, K., S. Chaen, E. Kamitsubo, T. Shimmen, and H. Sugi. 1990. Steady-state force velocity relation in the ATP-dependent sliding movement of myosin-coated beads on actin cables in vitro studied with a centrifuge microscope. *Proc. Natl. Acad. Sci. U. S. A.* 87: 7893–7897.
113. Edman, K., A. Mansson, and C. Caputo. 1997. The biphasic force-velocity relationship in frog muscle fibres and its evaluation in terms of cross-bridge function. *J. Physiol.* (*Lond.*). 503:141–156.
114. Saeki, Y., M. Kawai, and Y. Zhao. 1991. Comparison of crossbridge dynamics between intact and skinned myocardium from ferret right ventricles. *Circ. Res.* 68:772–781.
115. Kawai, M., and P. Brandt. 1980. Sinusoidal analysis: a high resolution method for correlating biochemical reactions with physiological processes in activated skeletal muscles of rabbit, frog and crayfish. *J. Muscle Res. Cell Motil.* 1:279–303.
116. Rossmanith, G. H., J. F. Y. Hoh, A. Kirman, and L. J. Kwan. 1986. Influence of V_1 and V_3 isomyosins on the mechanical behavior of rat papillary muscle as studied by pseudorandom binary noise-modulated length perturbations. *J. Muscle Res. Cell Motil.* 7:307–319.
117. Mercadier, J., P. Bouveret, L. Gorza, S. Schiaffino, W. Clark, R. Zak, B. Swynghedauw, and K. Schwartz. 1983. Myosin isoenzymes in normal and hypertrophied human ventricular myocardium. *Circ. Res.* 53:52–62.
118. Kawai, M., Y. Saeki, and Y. Zhao. 1993. crossbridge scheme and the kinetic constants of elementary steps deduced from chemically skinned papillary and trabecular muscles of the ferret. *Circ. Res.* 73:35–50.
119. Shibata, T., W. C. Hunter, and K. Sagawa. 1987. Dynamic stiffness of barium-contractured cardiac muscles with different speeds of contraction. *Circ. Res.* 60:770–779.
120. Shibata, T., W. C. Hunter, A. Yang, and K. Sagawa. 1987. Dynamic stiffness measured in central segment of excised rabbit papillary-muscles during barium contracture. *Circ. Res.* 60:756–769.
121. Ruf, T., H. Schulte-Baukloh, J. Ludemann, H. Posival, F. Beyersdorf, H. Just, and C. Holubarsch. 1998. Alterations of cross-bridge kinetics in human atrial and ventricular myocardium. *Cardiovasc. Res.* 40: 580–590.
122. Campbell, K. B., M. Chandra, R. D. Kirkpatrick, B. K. Slinker, and W. C. Hunter. 2004. Interpreting cardiac muscle force-length dynamics using a novel functional model. *Am. J. Physiol.* 286: H1535–H1545.
123. Mulieri, L. A., W. Barnes, B. J. Leavitt, F. P. Ittleman, M. M. LeWinter, N. R. Alpert, and D. W. Maughan. 2002. Alterations of

myocardial dynamic stiffness implicating abnormal crossbridge function in human mitral regurgitation heart failure. *Circ. Res.* 90: 66–72.

124. Berman, M. R., J. N. Peterson, D. T. Yue, and W. C. Hunter. 1988. Effect of isoproterenol on force transient time course and on stiffness spectra in rabbit papillary-muscle in barium contracture. *J. Mol. Cell. Cardiol.* 20:415–426.
125. Backx, P. H., and H. ter Keurs. 1988. The force response to sudden length changes in rat myocardium. *Biophys. J.* 53:167a.
126. Barany, M. 1967. ATPase activity of myosin correlated with speed of muscle shortening. *J. Gen. Physiol.* 50:197–218.
127. Fujita, H., and M. Kawai. 2002. Temperature effect on isometric tension is mediated by regulatory proteins tropomyosin and troponin in bovine myocardium. *J. Physiol.* (*Lond.*). 539:267–276.
128. Kentish, J. C. 1991. Combined inhibitory actions of acidosis and phosphate on maximum force production in rat skinned cardiac muscle. *Pflueg. Arch. Eur. J. Physiol.* 419:310–318.
129. Saeki, Y., K. Sagawa, and H. Suga. 1980. Transient tension responses of heart muscle in Ca^{2+} contracture to step-length changes. *Am. J. Physiol.* 238:H340–H347.
130. Hancock, W. O., D. A. Martyn, L. L. Huntsman, and A. M. Gordon. 1996. Influence of Ca^{2+} on force redevelopment kinetics in skinned rat myocardium. *Biophys. J.* 70:2819–2829.
131. Rossmanith, G. H., and O. B. Tjokorda. 1998. Relationships between isometric and isotonic mechanical parameters and cross-bridge kinetics. *Clin. Exp. Pharmacol. Physiol.* 25:522–535.
132. de Beer, E. L., A. E. Bottone, J. van der Velden, and E. E. Voest. 2000. Doxorubicin impairs crossbridge turnover kinetics in skinned cardiac trabeculae after acute and chronic treatment. *Mol. Pharmacol.* 57:1152–1157.
133. Janssen, P. M. L., and P. P. de Tombe. 1997. Uncontrolled sarcomere shortening increases intracellular Ca^{2+} transient in rat cardiac trabeculae. *Am. J. Physiol.* 41:H1892–H1897.
134. Brutsaert, D. L., and S. U. Sys. 1989. Relaxation and diastole of the heart. *Physiol. Rev.* 69:1228–1315.
135. Box, G. E. P. 1978. Statistics for Experimenters: An Introduction to Design, Data Analysis, and Model Building. Wiley, New York.
136. Hancock, W. O., D. A. Martyn, and L. L. Huntsman. 1993. Ca^{2+} and segment length dependence of isometric force kinetics intact ferret cardiac muscle. *Circ. Res.* 73:603–611.
137. Sugi, H., and T. Tameyasu. 1979. Origin of the instantaneous elasticity in single frog muscle fibers. *Experientia* (*Basel*). 35:227–228.
138. Baker, A.J., V.M. Figueredo, E.C. Keung, and S.A. Camacho. 1998. Ca^{2+} regulates the kinetics of tension development in intact cardiac muscle. *Am. J. Physiol.* 275:H744–H750.
139. Wolff, M.R., K.S. McDonald, and R.L. Moss. 1995. Rate of tension development in cardiac muscle varies with level of activator calcium. *Circ. Res.* 76:154.
140. Rassier, D.E., and W. Herzog. 2004. Active force inhibition and stretch-induced force enhancement in frog muscle treated with BDM. *J. Appl. Physiol.* 97:1395–1400.
141. Rassier, D. E., and W. Herzog. 2004. Considerations on the history dependence of muscle contraction. *J. Appl. Physiol.* 96:419–427.
142. Takimoto, E., D. G. Soergel, P. M. L. Janssen, L. B. Stull, D. A. Kass, and A. M. Murphy. 2004. Frequency- and afterload-dependent cardiac modulation in vivo by Troponin I with constitutively active protein kinase A phosphorylation sites. *Circ. Res.* 94:496–504.
143. Kentish, J. C., and A. Wrzosek. 1998. Changes in force and cytosolic Ca^{2+} concentration after length changes in isolated rat ventricular trabeculae. *J. Physiol.* (*Lond.*). 506:431–444.
144. Perez, N. G., K. Hashimoto, S. McCune, R. A. Altschuld, and E. Marban. 1999. Origin of contractile dysfunction in heart failure—calcium cycling versus myofilaments. *Circulation.* 99:1077–1083.
145. Stehle, R., M. Kruger, P. Scherer, K. Brixius, R. H. G. Schwinger, and G. Pfitzer. 2002. Isometric force kinetics upon rapid activation and relaxation of mouse, guinea pig and human heart muscle studied on the subcellular myofibrillar level. *Basic Res. Cardiol.* 97:1435–1803.
146. Belus, A., N. Piroddi, and C. Tesi. 2003. Mechanism of cross-bridge detachment in isometric force relaxation of skeletal and cardiac myofibrils. *J. Muscle Res. Cell Motil.* 24:263–269.
147. Hunter, P., N. Smith, J. Fernandez, and M. Tawhai. 2005. Integration from proteins to organs: the IUPS Physiome Project. *Mech. Ageing Dev.* 126:187–192.
148. Cuellar, A. A., C. M. Lloyd, P. F. Nielsen, M. D. B. Halstead, D. P. Bullivant, D. P. Nickerson, and P. Hunter. 2003. An overview of CellML 1.1, a biological model description language. *Trans. Soc. Model. Simu. Int.* 79:740–747.
149. de Tombe, P. P., and H. ter Keurs. 1991. Lack of effect of isoproterenol on unloaded velocity of sarcomere shortening in rat cardiac trabeculae. *Circ. Res.* 68:382–391.
150. McDonald, K. S., M. R. Wolff, and R. L. Moss. 1998. Force-velocity and power-load curves in rat skinned cardiac myocytes. *J. Physiol.* (*Lond.*). 511:519–531.
151. Fujita, H., D. Sasaki, S.I. Ishiwata, and M. Kawai. 2002. Elementary steps of the cross-bridge cycle in bovine myocardium with and without regulatory proteins. *Biophys. J.* 82:915–928.